Article:
Haruna, MA orcid.org/0000-0003-3504-1876, Gardy, J orcid.org/0000-0003-1806-4056, Yao, G orcid.org/0000-0002-3292-2152 et al. (3 more authors) (2020) Nanoparticle modified polyacrylamide for enhanced oil recovery at harsh conditions. Fuel, 268. 117186. ISSN 0016-2361

https://doi.org/10.1016/j.fuel.2020.117186

Nanoparticle Modified Polyacrylamide for Enhanced Oil Recovery at Harsh Conditions

Maje Alhaji Haruna[1], Jabbar Gardy[1], Guice Yao[1], Zhongliang Hu[1], Nicole Hondow[1], Dongsheng Wen[1,2*]

[1] School of Chemical and Process Engineering, University of Leeds, Leeds, LS2 9JT UK

[3] School of Aeronautic Science and Engineering, Beihang University, Beijing, 100191, China

[*] (D.W.) ☎: +44(0)113 343 1299; ✉: d.wen@leeds.ac.uk and d.wen@buaa.edu.cn

Abstract

Silicon dioxide (SiO_2) nanoparticles (NPs) have been recently proposed to boost the performance of polyacrylamide (PAM) for enhanced oil recovery (EOR) applications. However, SiO_2/PAM nanocomposites tend to agglomerate or even sediment under harsh conditions such as high temperature-high salinity (HT-HS), which greatly decreases the potential for future field applications. In this work, SiO_2 NPs were modified using (3-aminopropyl) triethoxysilane (M_SiO_2) to create positively charged active groups that enhanced a stronger interaction with PAM functional groups, leading to high dispersion stability. Three samples including M_SiO_2/PAM, SiO_2/PAM and NP-free PAM were synthesised *in-situ* via free radical polymerisation, and their thermal stability, rheological properties and the effect of aging time were studied. It was found that M_SiO_2 could inhibit thermal degradation of the polymer and safeguard its backbone to prevent the polymer molecule from rupture. As a result, M_SiO_2/PAM exhibited much better thermal stability in harsh environments. After 90 days of aging, SiO_2/PAM and NP-free PAM had 45 and 78% viscosity reduction; whereas only 10% reduction was observed in the case of M_SiO_2/PAM. Additionally, core-flooding experiments showed that M_SiO_2/PAM solutions produced more oil recovery than those from SiO_2/PAM and NP-free PAM solutions at HT-HS condition.

Keywords: Enhanced oil recovery; Polymer flooding, Polyacrylamide; Silicon dioxide nanoparticles; High temperature and high salinity; Stability

Graphical abstracts:

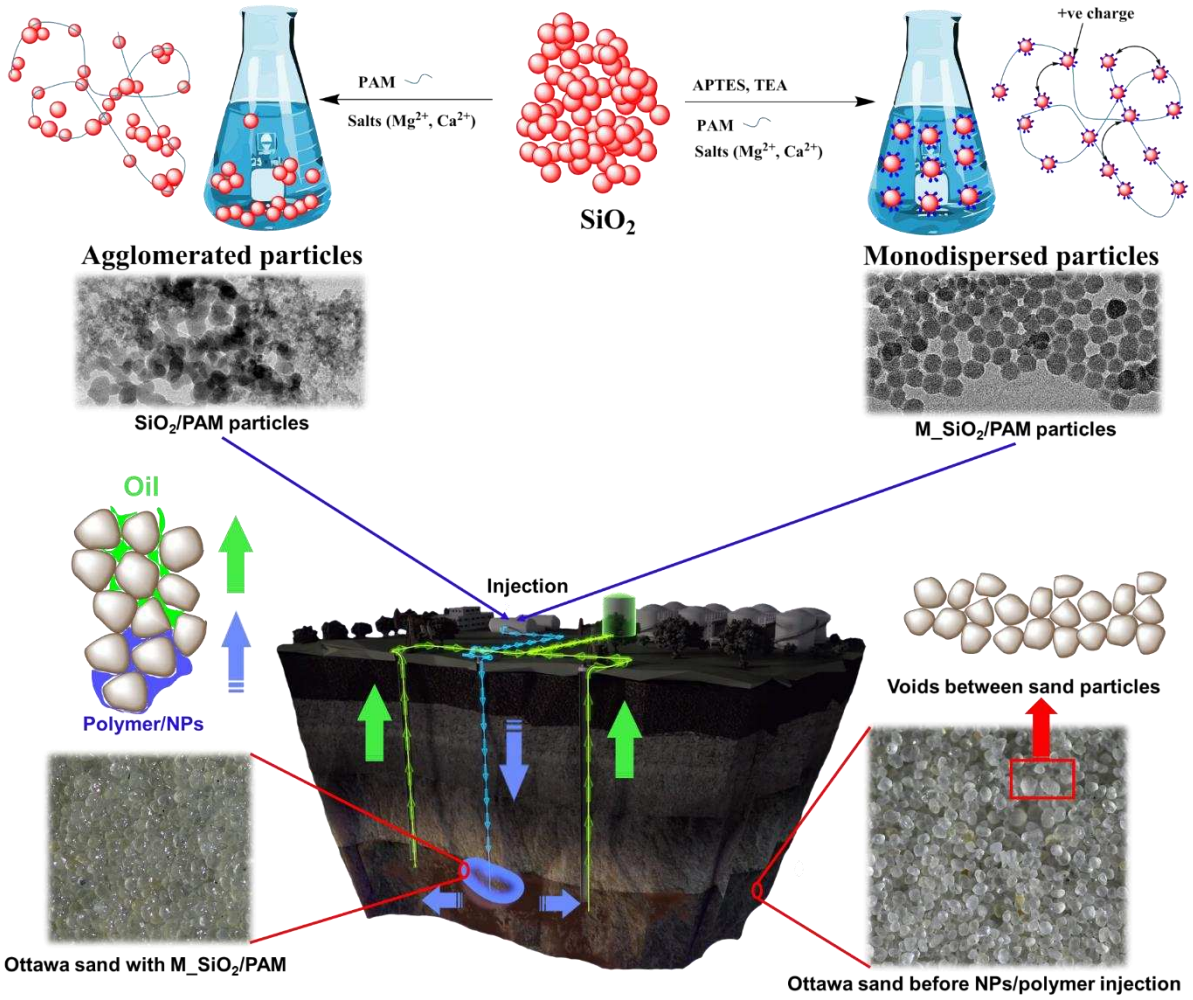

1. Introduction

Energy is the single most essential issue that the world is currently facing [1]. Oil still remains as a major source of primary energy, and enhanced oil recovery (EOR) is critical to meet our energy demand. Polymer flooding (PF) is widely applied as chemical EOR technique for increasing the reservoir sweep efficiency [2-5], by altering the mobility ratio between oil and displacing fluid to reduce viscous fingering. Polyacrylamide (PAM) and its derivatives as viscosifying agents have been widely used for PF application [6, 7], and could provide more oil recovery up to 60% [8]. However, the efficiency of PAM flooding is affected by a number of factors, including i) pore throats blockage because of the polymer aggregation [9, 10], ii) polymer degradation under harsh conditions such as high temperature-high salinity (HT-HS) and extreme pH, thereby lowering the displacing fluid's viscosity [11-15], and iii) polymer adsorption onto the surface of the reservoir rock, making the process expensive [16, 17].

Chemical modification [18-20] have been implemented to address the limitations of EOR polymers, but comes with many other problems including low solubility, high chemical cost and elevated resistance factor. Natural or synthetic inorganic materials have been also used to fill the conventional polymers to enhance their performance and has become economically viable [21]. On the other hand, these added fillers bring many other problems for the application resulting in opacity, brittleness and weight increase [21, 22].

In recent years, nanoparticles (NPs) have been used as an alternative technique to address the challenges facing EOR [22-28]. NPs exhibit exceptional properties owing to the small size and large surface area. Ability to manipulate NPs surface properties, such as being hydrophobic or hydrophilic or amphiphilic in nature, as well as ability to alter the surfaces charges from positive or negative charge and vice versa [29-32]. With these advantages of NPs, when added to the EOR displacement fluids it can alter the wettability state of the rock [33-35], improve the rheological properties [26, 36, 37], and lower the interfacial tension [37-39], etc. NPs can

also lower the adsorption of polymer or surfactant on reservoir rock as well [30]. Similarly, a number of studies have shown that addition of NPs could enhance the thermal stability of PAM [40-42].

SiO_2 NPs have been the most widely investigated to boost the performance of PAM in EOR applications owing to their availability and easy surface functionalisation nature [26, 36, 43-49]. Our recent work has shown that SiO_2 NPs could form strong interactions with PAM via hydrogen bond between silanol functionalities of SiO_2 and PAM amide groups [26]. It was also observed that the interaction could happen through carbonyl groups of the PAM acting as physical cross-linker between macromolecules, thereby reinforcing the structure of the polymer to provide better mechanical properties [46, 47, 50].

For EOR applications, however, the stability of these nanocomposites have to be examined under HT-HS conditions. Our recent study show that under a high ionic strength of brine, the SiO_2 NPs start to agglomerate causing large numbers of silanol groups that shelter the SiO_2 surface to create aggregates of NPs. The lack of good SiO_2 dispersion were likely due to their preferred face-to-face stacking in agglomerated/aggregated tactoids [48], which leads to severe agglomeration and sedimentation in a harsh environment [51]. In addition, when SiO_2 NPs and a polymer are mixed, it takes a long time to form well-dispersed mixture, which greatly decrease the potential field application of NP-based systems. Similar observation was also reported in the literature [49]. It has been shown that the hydrophilic nature of SiO_2 NPs decreased the physical strength to interact with the polymer matrix that has hydrophobic structure, making the dispersion more difficult [52, 53].

Aiming to address these two challenges facing SiO_2/PAM dispersion, this work proposed a novel surface modification approach to produce well-dispersed SiO_2 dispersion, and use them for *in situ* synthesis of PAM to form stable nanocomposite. Several approaches, including

grafting of polymers, chemical (through covalent bonding) and physical (through physisorption) strategies are previously used for surface modification of NPs [54, 55], but all have different limitations. In this work, SiO_2 NPs were modified by functionalising the surface with (3-aminopropyl)triethoxysilane (M_SiO_2) to create positively charged active sites so as to produce monodispersed particles. In addition to conventional hydrogen bonds, positive charged surfaces allow strong coordination bonds with the PAM's negative charged side chain, reinforcing its stability under HS conditions. Three copolymers of M_SiO_2/PAM, SiO_2/PAM and NP-free PAM were synthesised *in situ* via a free radical polymerisation process of 2-acrylamido-2-methyl-1-propanesulfonic acid and acrylamide (APSA and AA) monomers. The effect of NP-free PAM, SiO_2/PAM and M_SiO_2/PAM on the thermal stability, long term aging at HT-HS condition was investigated. A pilot scale of core-flooding investigations were also conducted to investigate their potential use for EOR.

2. Materials and methodologies

2.1. Materials

2-Acrylamido-2-methyl-1-propanesulfonic acid (APSA, 99%), acrylamide (AA, 99%), 4-4'-azo-bis-4-cyanopentanoic acid (ACPA) monomers and SiO_2 NPs (12 nm, ≥99.0% purity) were obtained from Sigma-Aldrich. Polydimethylsiloxane, (3-aminopropyl)triethoxysilane (APTES, 99%), trimethylsiloxy terminated, high viscous silicon oil (M.Wt. 9000) were purchased from Alfa Aesar and triethylamine (TEA, 99%) was acquired from VWR International. The obtained reagents and chemicals were used directly without any extra purification.

2.2. Synthesis methodologies

2.2.2. Synthesis of amino-functionalised nanosilica

Modified SiO_2 (M_SiO_2) was obtained by functionalising SiO_2 NPs with APTES. Firstly, 6.0 g of SiO_2 was put in a clean container followed by the addition of 100 ml ethanol, and then

stirred at ambient temperature for 2 h. Different APTES concentrations (see **Table 1**) was dissolved in 100 ml (90/10, v/v) of ethanol/water. Subsequently, the dispersion of SiO_2 and solution of APTES were introduced into a container, 2.5 ml TEA was added to the mixture and stirred for 4 h at 80 °C to achieve the modification. The resulting material was separated using centrifuge and then rigorous washing was performed using ethanol. The dried product was obtained in a *vacuo* after 24 h at 80 °C and the M_SiO_2 suspension was obtained and sealed in a clean container. **Table 1** shows five different synthesised M_SiO_2 samples.

Table 1. Properties of SiO_2 and M_SiO_2 samples

Sample code	NP (g)	APTES (g)	Elemental compositions (wt. %)*			Amino group content (%)**	Zeta potential (mV)
			C	H	N		
SiO_2	6.0	0.0	0.00	0.00	0.00	0.00	-20.2
$MSiO_2$-1	6.0	0.4	4.88	1.22	1.64	4.6	-24.7
$MSiO_2$-2	6.0	0.8	5.15	1.25	1.70	4.8	-32.4
$MSiO_2$-3	6.0	1.6	5.61	1.31	1.77	5.8	-34.8
$MSiO_2$-4	6.0	2.4	6.09	1.40	1.85	6.4	-37.3
$MSiO_2$-5	6.0	3.2	6.20	1.41	2.07	7.3	-44.7

* Elemental compositions for all samples were measured using CHNS-O analyser ** % of amino groups in all samples was quantified from TGA curves.

2.2.2. Synthesis of polymer and NPs/polymer composites

The polymer and NPs/polymer composites were prepared *in situ* through a free-radical polymerisation. The mixture of AA and APSA monomers, with the amount in gram as shown in **Table 2** was dissolved in 80 ml deionised water. The NPs dispersion was obtained by dispersing 0.5 g of either SiO_2 or M_SiO_2 NPs in 40 ml of deionised water and sonicated at ambient temperature for 30 min. The monomer solution along with NPs dispersion were poured into a three neck bottom glass container and followed by 30 min stirring under inert atmosphere using a magnetic stirrer at 200 RPM. ACPA was added (10 mg) as an initiator to trigger the free-radical polymerisation reaction and the reaction was then gently mixed, using a magnetic stirrer, for 6 h at 80 °C under reflux. The polymerisation reaction was entirely performed under nitrogen gas. For investigation, one NP-free PAM were synthesised in a similar way as a

contrast sample as shown in **Table 2**. In order to conduct the rheology and core flooding test at harsh condition, the prepared M_SiO_2/PAM, SiO_2/PAM, and NP-free PAM was dispersed in two types of brines: (1) standard American Petroleum Institute brine (AB) and (2) formation brine (FB). FB can be found in the largest oil well in the world known as the Ghawar field found in Saudi Arabia [56]. The composition and relative weight percent of the salt are provided in **Table 3**.

Table 2. Properties of polymer and polymer nanocomposite

Sample	Monomers (g)		NPs type/ amount (g)	$M_{wt,GPC}$ (g/mol)	Elemental compositions (wt. %)					Zeta potential (mV)
	AA	APSA			N	C	H	S	O	
NP-free PAM	3.75	3.75	---	696575	11.91	41.82	6.31	5.93	34.03	-28.7
SiO_2/PAM	3.75	3.75	SiO_2/0.6	---	12.07	40.98	7.11	7.22	32.62	-29.9
M_SiO_2/PAM	3.75	3.75	M_SiO_2/0.6	---	11.91	40.65	6.19	6.94	34.31	-49.6

Table 3: Variation of the amount of salt

Salt species	Formation brine (FB) (%)	API Brine (AB) (%)
$BaCl_2$	0.001	/
$NaHCO_4$	0.005	/
Na_2SO_4	0.006	/
$MgCl_2.6H_2O$	1.3	/
$CaCl_2.2H_2O$	5.0	2
NaCl	7.5	8

2.3. Characterisation of nanoparticles and hybrid systems

Chemical composition was determined on elemental (CHNS-O) analyser (Thermo Scientific FLASH 2000 CHNS-O Analyser). The particle size distribution (PSD) and zeta potential were measured using a Malvern Nanosizer based on dynamic light scatting (DLS) method. The stability of M_SiO_2 over sedimentation and flocculation behaviour was performed using a dispersion analyser centrifuge (LUMiSizer, Lum GmbH, Germany) to record the near-infrared (NIR) light transmission during the centrifugation processes. This multi-sampler analytical centrifuge can reveal instantaneously the differences in the particle concentration by transmitting NIR-light through the samples length and allow the measurement of the extinction

profiles during centrifugation. The nuclear magnetic resonance (NMR) analysis of polymer was obtained on a JEOL-600 NMR spectrometer using D_2O as a solvent. The TGA/DSC-3 Mettler Toledo star^e system was used for the thermal stability analysis. The system was programmed to heat between the ranges of 35 and 900 °C with an interval of 10 °C/min, the system was operated under constant flow rate of nitrogen gas at 50 ml/min. The amount of the APTES loaded on the NPs was calculated from the data obtained on the TGA weight loss ranging between 400 and 650 °C. The functionality of the samples was analysed by attenuated total reflection-Fourier transform infrared (ATR-FTIR, Nicolet iS10). The data was collected within the range of wavenumber between 400 and 4000 cm^{-1} at a spectral resolution of 4 cm^{-1}. A cold-field emission scanning electron microscope (CFE-SEM, SU8230 Hitachi, Leeds Electron Microscopy and Spectroscopy Centre, UK) operated at 2 kV for imaging and 15 kV for spectroscopy and transmission electron microscope operated at 300 kV (TEM, FEI Titan Themis^3 300 with a Gatan OneView, LEMAS Centre, UK) were used to observe the surface morphology. The SEM was coupled with an energy dispersive X-ray spectrometer (EDX, Oxford Aztec 80 mm^2 X-Max SDD detector) and was used to identify the elemental compositions and locations. The samples for TEM were prepared via the method of Hondow *et al.* [57] to ensure that the nanoparticle dispersion state was captured. Gel permeation chromatography (Agilent Technologies Infinity 1260 MDS, GPC) was employed for polymer molecular weight determination. 0.1 M $NaNO_3$ were used as liquid phase for analysing the molecular weight and polydispersity of the polymer. A 0.22 μm pore size hydrophilic GVWP membrane was used to filter the sample before injection. A TA discovery hybrid rheometer (DHR-2) was employed to measure the shear and dynamic rheological properties. The measurement was conducted using cone and plate geometry having a 0.53 mm as pre-set gap. During the measurement the measuring geometry was sealed with a plastic ring solvent trap to minimise water evaporation. Throughout the measurement advanced Peltier setup were applied

to control the temperature. The flow property of the material was studied by steady shear sweep analysis to record the viscosity (η) against shear rates (γ). The loss modulus (G") and the storage modulus (G') were obtained at a range of angular frequency by measuring the dynamic frequency sweep in the linear viscoelastic regions to determine the viscoelastic properties of the materials.

2.4. Effect of aging and high temperature degradation

In a polymer flooding process, injection fluid stays for long period of times in the reservoir under severe conditions which include HT-HS before reaching the oil, therefore it is imperative to consider the effect of aging as a benchmark of understanding the capability of displacing fluid. In this work, 0.1 wt. % of NP-free PAM, SiO_2/PAM and M_SiO_2/PAM were prepared and aged in a sealed container under simulated oil field conditions. The apparent viscosity (AV) of each aged sample was measured after 24 h (1 day), followed by 10, 20, 30, 60 and 90 days, respectively. The relative viscosity (RV) was then calculated from Eqn. 1.

$$RV = \eta_t/\eta_0 \times 100\% \qquad \text{Eqn. (1)}$$

Where η_t represent apparent viscosity of the aged sample (mPa·s) (at particular day) and η_0 is the apparent viscosity at zero day aging.

2.5. Core-flooding investigation

To understand the ability of each solution in EOR, core-flooding investigation were carried out under HT-HS conditions, the calculated parameters are shown in **Table 4**. A stainless steel column with inner diameter of 2.5 cm and length of 70 cm was packed with Ottawa sand by conducting a series of rigorous wet-packing procedures to calculate relatively constant geometry and hydrodynamic values such as porosity and permeability. Before the EOR evaluation, NP-free PAM, SiO_2/PAM and M_SiO_2/PAM were stored for 90 days at 80 °C. The core holder containing packed sand was saturated with the brine at a flow rate of 2 ml/min

using a piston pump (Core-Palmer Instrument Co. Ltd, series I) to make sure the column was saturated thoroughly and grant sufficient interval for sand grain deposition. A KDS 410, KD Scientific Incorporated, USA syringe pump was employed to saturate the packed sand with viscous silicon oil at the speed of 0.5 ml/min. Three (3) pore volumes (PV) of simulated brine were injected as secondary oil recovery with rate of flow equal to 0.5 ml/min. After this tertiary recovery was executed by injecting 30 ml of displacing sample at a flow rate of 0.5 ml/min. Around 20 ml of brine was also injected as chased water at the same flow rate. A 50 ml granulated cylinder with 0.1 ml division was used to collect the effluent liquid and recovered oil to be able to actualize the amount of oil recovery. The total amount of oil recovered by each sample were recorded by calculating the difference between water flooding and secondary flooding. The target temperature of the controller was kept at 85 °C during the experiment using the three K-type thermocouples (5TC-TT-K-36-36, a precision of ±0.5 K and a diameter of 0.13 mm Omega) connected to the both ends and across the middle of the steel packed column **(Fig. 1).** A 150 psi, Omega Engineering Ltd pressure transducer, was applied for measuring the pressure drop whilst performing the experiments. EZ-ZONE PM Integrated PID Model temperature controller system was used to supply and control heating to the setup. Throughout the experiment, the temperature and pressure were maintained at 85 ± 1.5 °C and ambient, respectively.

Table 4. Average values of the packed sands column properties.

Porous media properties	Values
Permeability (mD)	95 ± 19.1
Porosity (%)	37.9 ± 2.3
Pore volume (ml)	11.9 ± 08
Bulk volume (ml)	34.9 ± 1.1
Mass of dry sands (g)	53.5 ± 3.6
Liquid in the pore space (g)	13.1 ± 0.2
Temperature (°C)	85 ± 1.5

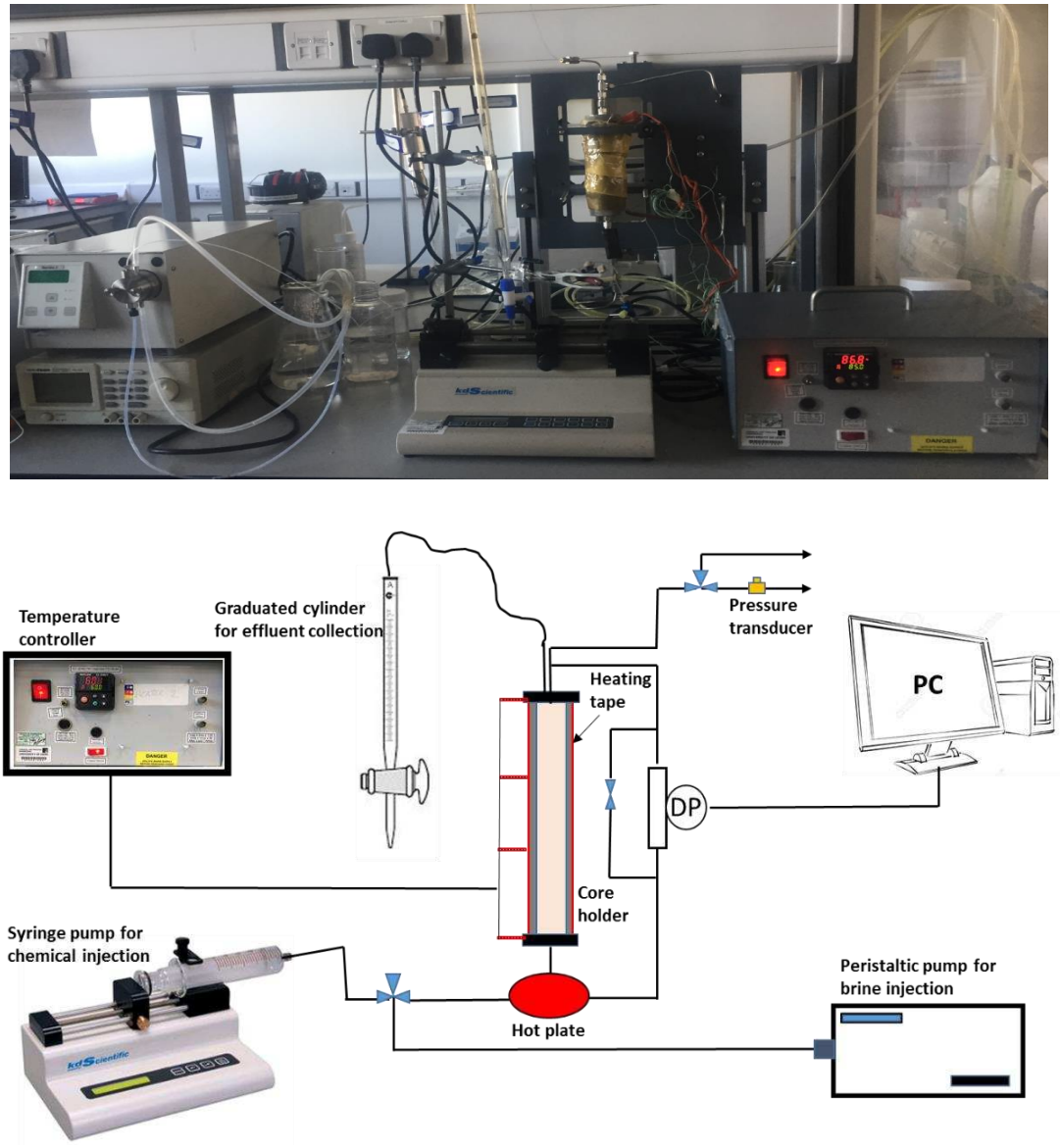

Figure 1. Experimental setup for flooding experiment (top), and Schematic illustration of core flooding system (bottom).

3. Results and discussion

3.1. Characterisation of M_SiO_2

Six different samples are shown in **Table 1,** one pure SiO_2 and five M_SiO_2 with various APTES concentrations. The elemental analysis results demonstrated an increase in the amino groups on the M_SiO_2 surface after the addition of different APTES content from M_SiO_2-1 to M_SiO_2-5. At the highest amount of APTES (3.2 g), the highest nitrogen content and

percentage of amino groups, is observed (7.2 wt. %). This could be due to the condensation reaction occurred on the surface of the M_SiO_2 causes by the presence of various APTES molecules as reported in the literature [58]. Similarly, the arrangement of some particular APTES molecules on the surface of M_SiO_2 could enhance the content of the functionalisation, which could at the same time promote the interaction between the polymer and NPs. Zeta potential of pure SiO_2 and series of modified particles were recorded in **Table 1**, the outcome shows that the higher the APTES content the higher the value of zeta potential, indicating that more APTES present with the particle promotes the particle stability by showing better dispersion properties. The hydrodynamic particle size distribution for pure SiO_2 and M_SiO_2-5 were measured by DLS following the particles dispersing in water as shown in **Fig. 2a**. The pure SiO_2 shows two peaks at around 44 and 335 nm, whereas M_SiO_2-5 displays only one peak at around 177 nm. This confirms that M_SiO_2 possesses better dispersion equity than the pure SiO_2 suspension. The aforementioned finding was also confirmed by investigating the morphology of the pure SiO_2 and M_SiO_2 using SEM and TEM analysis, where it shows clearly in **Fig. 2b** that pure SiO_2 has different size particles (bigger size labelled in red as shown in **Fig. 2b**), while M_SiO_2 shows homogenous mixture**.**

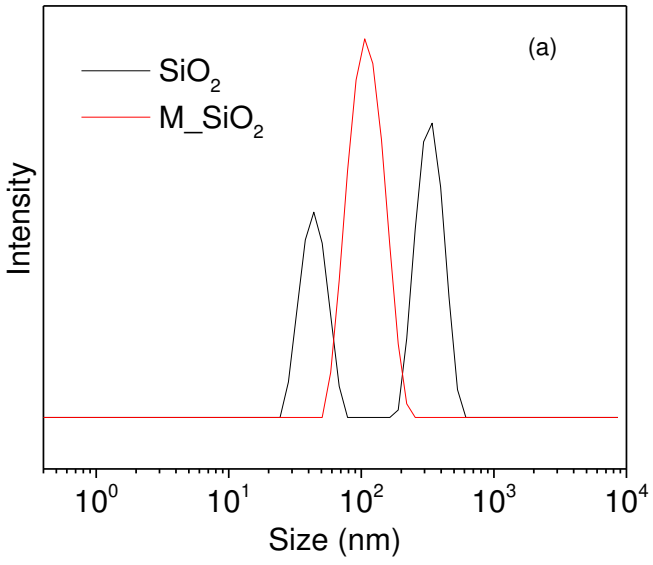

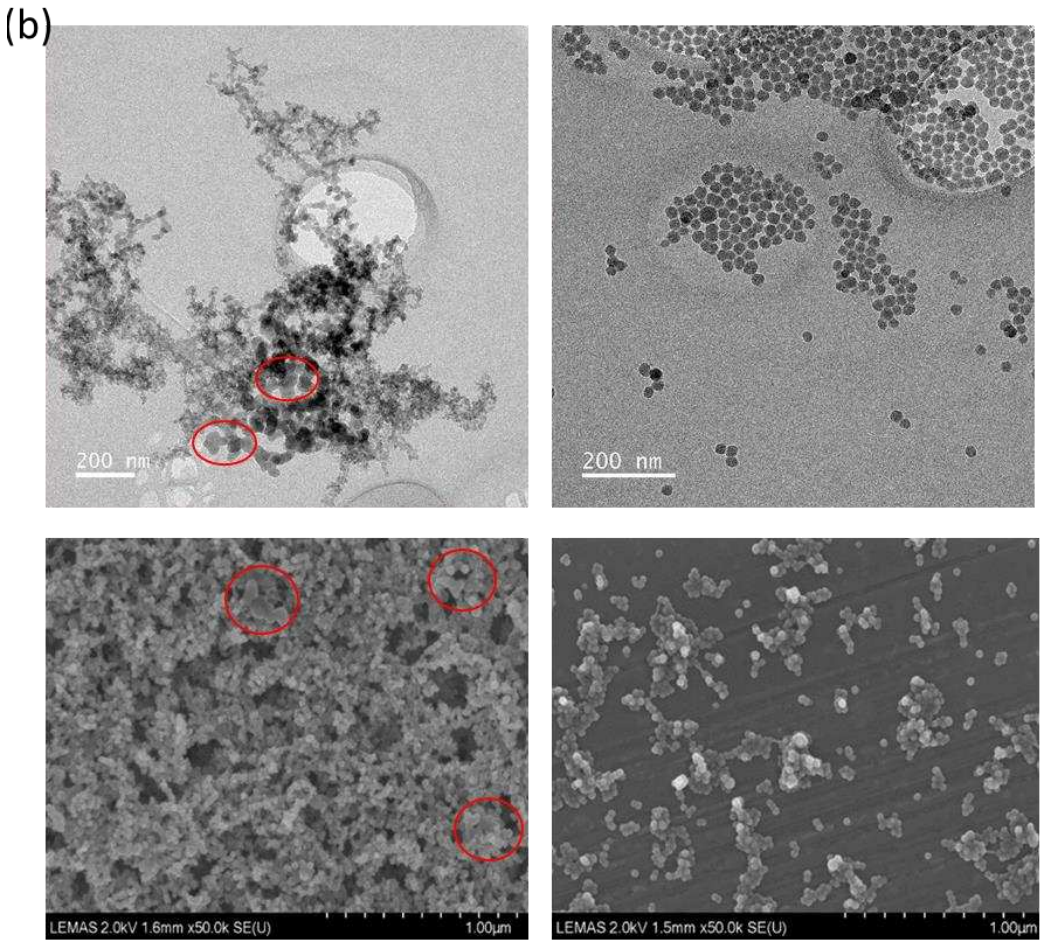

Figure 2. (a) DLS particle size distributions showing the difference in dispersion state after modification of the pure SiO_2 NPs and (b) TEM (top) / SEM (bottom) images of pure SiO_2 (left) and M_SiO_2 (right), with larger particles highlighted by red circles.

ATR-FTIR spectroscopy was employed for pure SiO_2 and the series of M_SiO_2 samples to analyse the behaviour of the chemical bonding as shown in **Fig. 3a**. The bands appearing at 3200 and 3583 cm^{-1} in M_SiO_2 represents the stretching vibration of N–H and O–H, respectively. The modified samples compared to pure SiO_2 shows extra new peaks at 1528 and 2931 cm^{-1} which are assigned to the N–H bending vibration and C–H stretching vibration, respectively. The peak at 1636 cm^{-1} represent the Si–O–H vibrations proving the existence of hydrogen bonding between the O molecule in SiO_2 and H atoms from the incorporated organic

components [26]. The FTIR spectra for all samples exhibit a deep Si–O–Si stretching vibration near 1078 cm^{-1} along with bending shift between 470 and 800 cm^{-1} [59].

Thermal analysis (TGA) of pure SiO_2 and M_SiO_2 with various APTES contents was performed with the heating range from 25 to 900 °C as shown in **Fig. 3b**, displaying similar results as reported in the literature [60-62]. The TGA curves demonstrated that SiO_2 displayed a small weight loss until 200 °C, which is related to desorption/evaporation of water molecules. Compared to the pure SiO_2 sample there are two stages of weight loss in M_SiO_2 samples, there was an initial weight loss at 450 °C confirming the attachment of APTES molecules on the surface of SiO_2, with a second stage of weight loss observed from 450 to 650 °C which is attributed to the decomposition of APTES molecules to form release of NH_3. The results were used to calculate the percentage of amine content in the NPs, and shows that the higher the APTES concentration the greater the amine contents present with the particle.

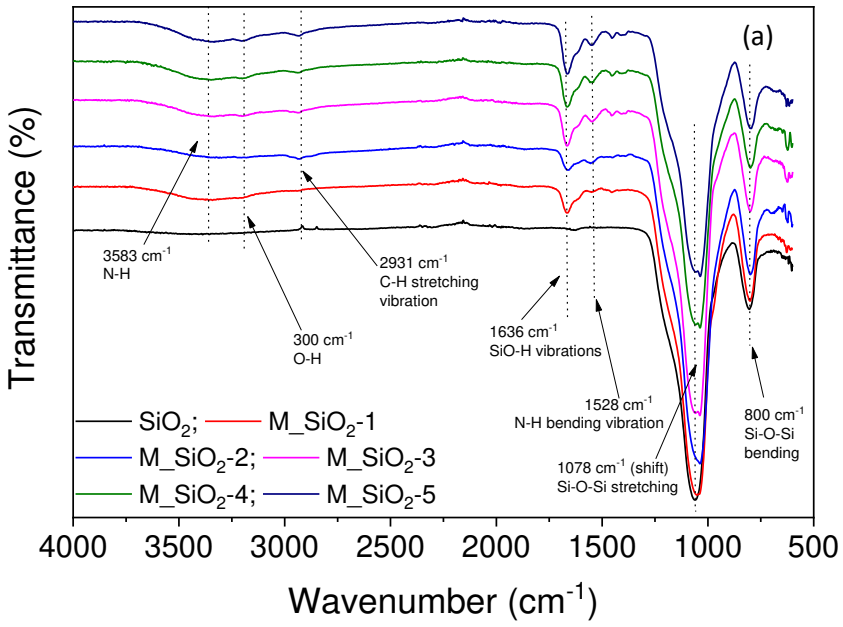

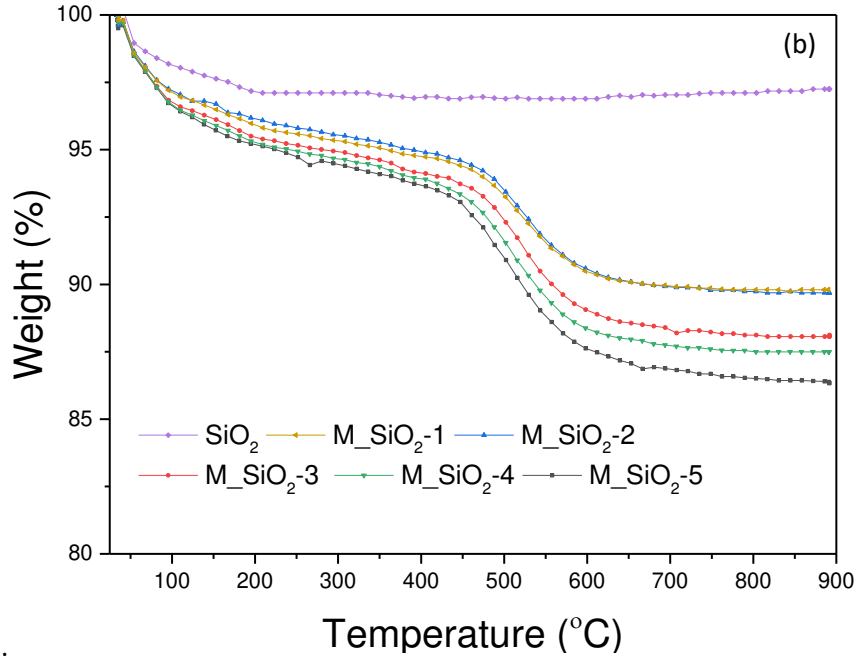

.....

Figure 3. (a) FTIR spectra of pure SiO_2, M_SiO_2-1, M_SiO_2-2, M_SiO_2-3, M_SiO_2-4 and M_SiO_2-5 **(b)** TGA profiles of pure SiO_2 and M_SiO_2 with different APTES contents.

3.2. Determining the best particle sample for making the composite.

The dispersion stability of the five modified silica's (M_SiO_2-1, M_SiO_2-2, M_SiO_2-3, M_SiO_2-4 and M_SiO_2-5) and pure SiO_2 was investigated to observe the sedimentation using LUMiSizer [63, 64]. The stability behaviour of pure SiO_2 and M_SiO_2 silica can be explained schematically as shown in **scheme 1**. For example, the pure SiO_2 NPs tend to aggregate into larger structures and settled down over short time. However, this make pure SiO_2 to create higher open particle bed structure which aggregated more by the applied centrifugal force. In contrast, M_SiO_2 are less likely to sediment because they are well dispersed as confirmed by DLS size distribution, TEM and SEM shown in **Fig. 2**. Consequently, the larger mass aggregates tents to sediment quickly when compared to well dispersed individual particles, which have longer sediment bed formation time. The examined particle packing behaviour in relation to applied centrifugal force is similar to the observation made by other researches [65-67], where the pressure-insensitive packed bed is formed by the NPs with the stable dispersion while a pressure-dependent network is created by aggregate NPs dispersion [67].

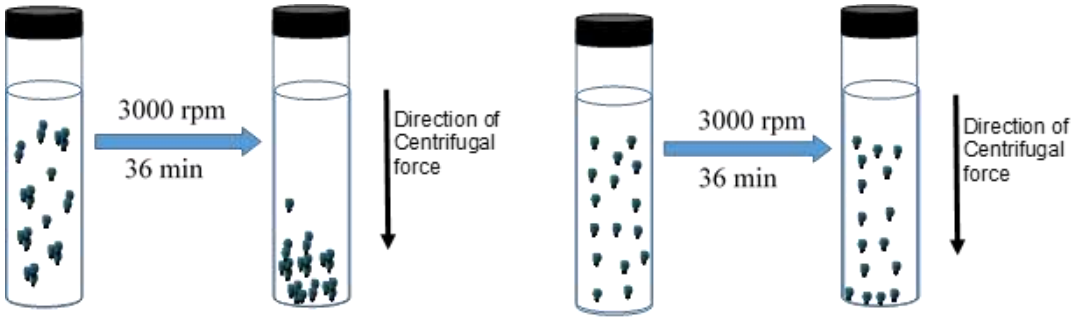

Scheme 1: Schematic illustration showing the effect of centrifugal force on the nature of sedimentation of (left) aggregated and precipitated pure SiO_2 and (right) Stable and well dispersed M_SiO_2.

To enable us evaluate the effects of functionalisation on SiO_2 stability using Lumisizer, about 0.5 ml of each particle dispersion was added to a polycarbonate capillary cell and centrifuged for 36 min duration at 3000 rpm (equivalent to 1 month in real conditions) [27]. Effect of different amount of APTES on the SiO_2 was used to observe the stability of NPs dispersion. **Fig. 4** shows the style at which the light is passing or transmitted across the test tube indicating that the M_SiO_2 has better stability compared to pure SiO_2 NPs. **Fig. 4a** indicate that pure SiO_2 shows higher bed sediment to around 65% transmission profile (red colour) illustrating a quick and faster settling of the particle to form an aggregate of larger structures, however, the bed sediment start to decrease to 58% transmission for M_SiO_2-1 as showing in **Fig. 4b**. More obvious decrease in sedimentation profile was observed in M_SiO_2-5 as illustrated in **Fig. 4b.** This effect of dispersion stability was confirmed by zeta potential, particle size distribution and SEM/TEM analysis as discussed in section 3.1. Moreover, prior to the analysis, the influence of NP type on the apparent viscosity (APV) was investigated using 0.1 wt. % of pure SiO_2 and M_SiO_2-5. The results show an increase in APV with the addition of APTES content from pure SiO_2 to M_SiO_2-5 (**Fig. 6a),** which is consistent with an increase in amino groups on the NP surface. Due to the high APV of M_SiO_2-5, different concentrations of both pure SiO_2 and M_SiO_2-5 were selected to examine the effect of particle concentrations, with the finding showing an increase in APV with increase in pure SiO_2 or M_SiO_2-5 concentration (**Fig. 6b**). **Fig. 5** shows the instability index of M_SiO_2 and pure SiO_2 containing APTES dispersion with

different concentrations. The results displayed that increasing the APTES contents make the stability of the suspension to increase, which is presumably occur as a results of the presence of positive charge (H^+) proton on the surface of M-SiO_2, thus providing a strong electrostatic repulsive force between functionalised particles and therefore leading to better stability.

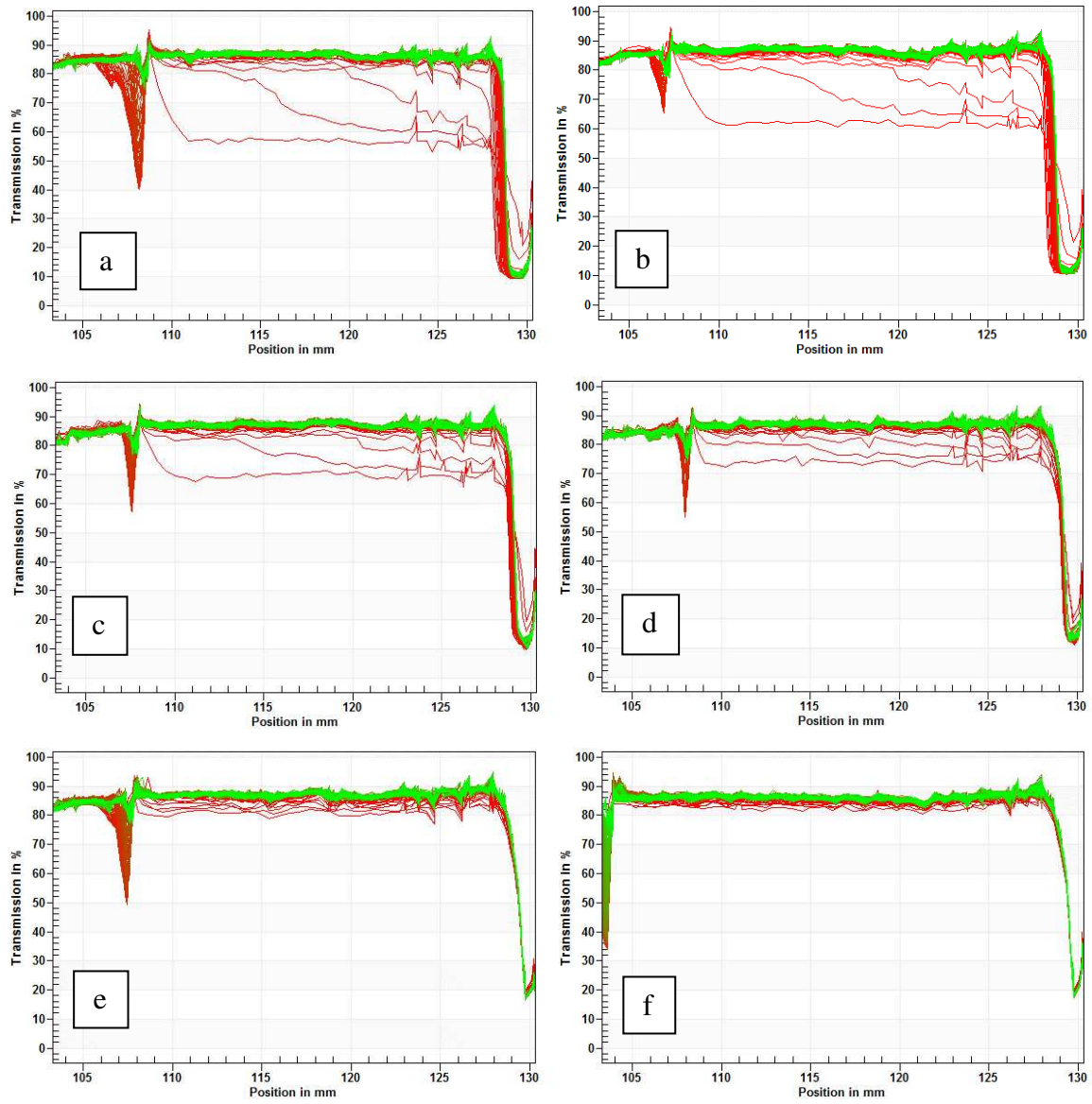

Figure 4. Styles of light transmission across the test tube for (a) pure SiO_2, (b) M_SiO_2-1, (c) M_SiO_2-2, (d) M_SiO_2-3, (e) M_SiO_2-4, (f) M_SiO_2-5 at the end of centrifuge process.

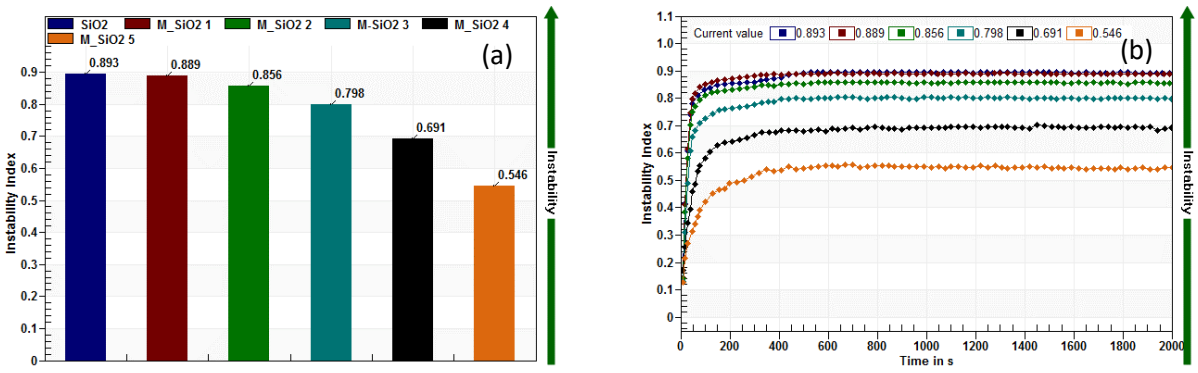

Figure 5. Instability index of SiO_2 and M_SiO_2 with different APTES (a) trend of centrifuge dispersion analyser for pure SiO_2 and M_SiO_2 with different APTES contents (b) stable immobile dispersions of pure SiO_2 and M_SiO_2 after 30 days at 85 °C.

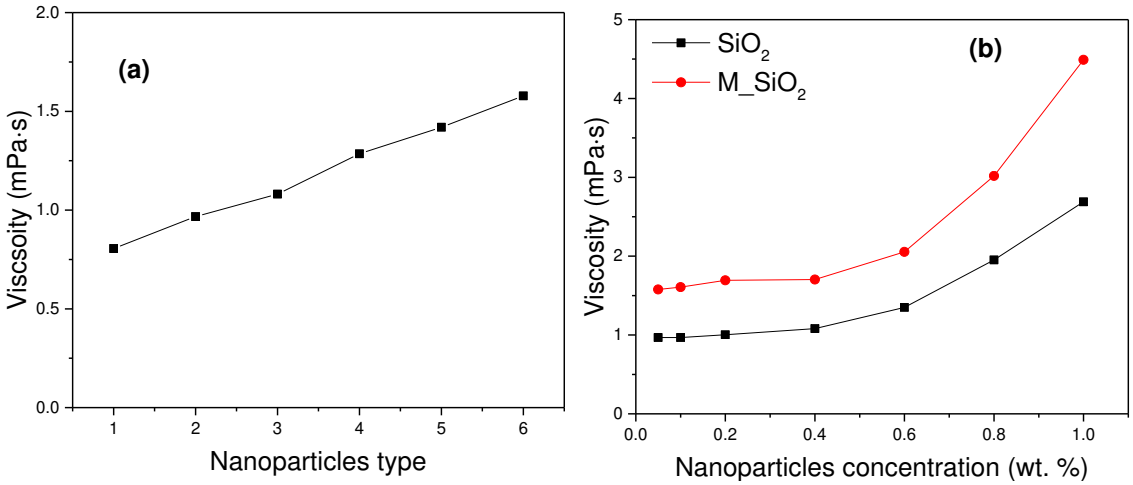

Figure 6. (a) Effect of NP type on the apparent viscosity and RV, and (b) viscosity as a function of pure SiO_2 and M_SiO_2-5 concentration (shear rate 1000 s^{-1} and T = 85 °C).

3.3. Characterisation of polymer and polymer/nanoparticles composites

Considering higher stability and high APV of M_SiO_2-5, it was selected as an inorganic constituent for the fabrication of NPs/PAM composites. Three samples were synthesised (NP-free PAM, SiO_2/PAM and M_SiO_2/PAM) via free radical polymerization to evaluate the effect of thermal stability. The formation of these synthesized polymers were examined by freeze-dried SEM, elemental analysis, TGA, ATR-FTIR and ^{1}H-NMR. The morphology of the freeze-dried polymer and polymer NPs dispersion were examined using SEM analysis. The results show the sponge-like structure of the NP-free PAM exhibiting a thick block with sparse pores

as shown in **Fig. 7a,** pure SiO_2 NPs addition shows there is a clear particle aggregation in polymer which results in flocculation and lack of proper dispersion and hence reduces the changes of obtaining highly stable material (**Fig. 7b**). Contrarily, the M_SiO_2/PAM shows characteristics filamentous structures with interconnecting pores promoting better dispersion stability where the APTES molecules induce an energetically favoured layer-by-layer to form a stable composite with 3D porous network having no obvious aggregation of the particles (**Fig. 7c**). It is interesting to know that the M_SiO_2/PAM composite creates a denser structure of the hybrid system; this is attributed to the formation of much stronger hydrogen bond interaction between the polar function group of PAM side chains and oxygen containing groups of the M_SiO_2. However, this could be also due to the increase amount of amino groups in the PAM following the addition of M_SiO_2. It can be observed that from the EDX maps (**Fig. 7b and c**) a more homogenous mixture of the elements (Si, C, N, O, and S) is present in M_SiO_2/PAM compared to SiO_2/PAM, which reaffirms the formation of stable composite material. The ^{1}H-NMR of the polymers is displayed in **Fig. 8**. The peak at 1.4 ppm is the methyl proton of the APSA unit, while that of methylene proton appears around 3.1-3.7 ppm. The peaks between 2.0-2.3 ppm indicate the existence of methane ($–CH_3$) protons in the polymer backbone. The peaks at 6.9 and 7.6 ppm attributed to the protons of C–H and R–CO–NH_2, respectively, revealing the formation of major polyacrylamide functional groups in the spectrum.

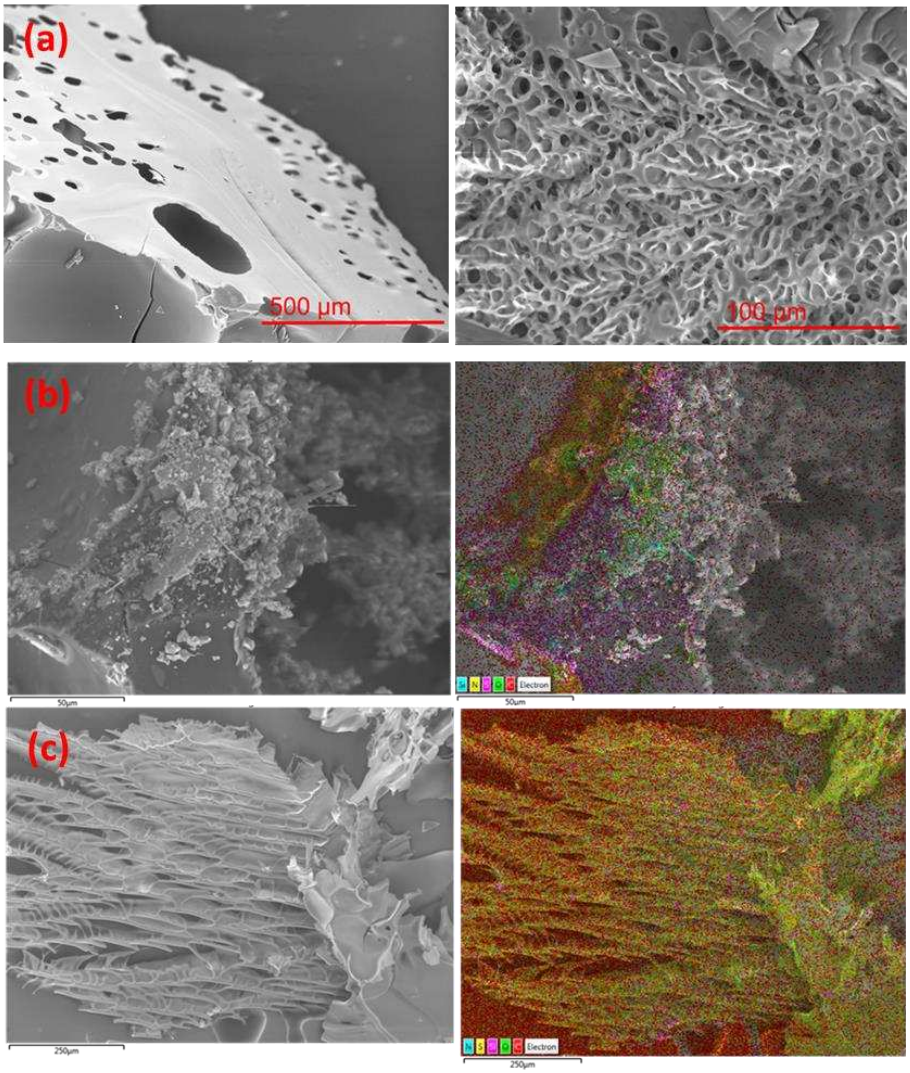

Figure 7. SEM images of the freeze-dried (a) NP-free PAM (b) SiO_2/PAM and (c) M_SiO_2/PAM.

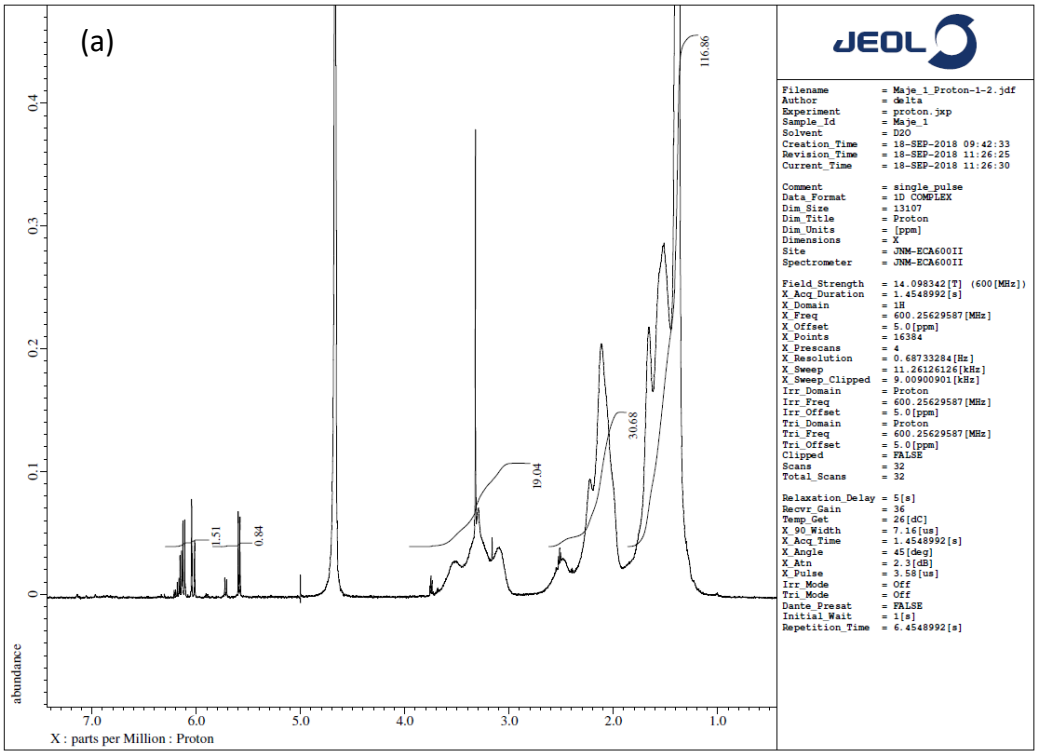
(a)
116.86
30.68
19.04
1.51
0.84
abundance
X : parts per Million : Proton
JEOL
Filename = Maje_1_Proton-1-2.jdf
Author = delta
Experiment = proton.jxp
Sample_Id = Maje_1
Solvent = D2O
Creation_Time = 18-SEP-2018 09:42:33
Revision_Time = 18-SEP-2018 11:26:25
Current_Time = 18-SEP-2018 11:26:30
Comment = single_pulse
Data_Format = 1D COMPLEX
Dim_Size = 13107
Dim_Title = Proton
Dim_Units = [ppm]
Dimensions = X
Site = JNM-ECA600II
Spectrometer = JNM-ECA600II
Field_Strength = 14.098342[T] (600[MHz])
X_Acq_Duration = 1.4548992[s]
X_Domain = 1H
X_Freq = 600.25629587[MHz]
X_Offset = 5.0[ppm]
X_Points = 16384
X_Prescans = 4
X_Resolution = 0.68733284[Hz]
X_Sweep = 11.26126126[kHz]
X_Sweep_Clipped = 9.00900901[kHz]
Irr_Domain = Proton
Irr_Freq = 600.25629587[MHz]
Irr_Offset = 5.0[ppm]
Tri_Domain = Proton
Tri_Freq = 600.25629587[MHz]
Tri_Offset = 5.0[ppm]
Clipped = FALSE
Scans = 32
Total_Scans = 32
Relaxation_Delay = 5[s]
Recvr_Gain = 36
Temp_Get = 26[dC]
X_90_Width = 7.16[us]
X_Acq_Time = 1.4548992[s]
X_Angle = 45[deg]
X_Atn = 2.3[dB]
X_Pulse = 3.58[us]
Irr_Mode = Off
Tri_Mode = Off
Dante_Presat = FALSE
Initial_Wait = 1[s]
Repetition_Time = 6.4548992[s]

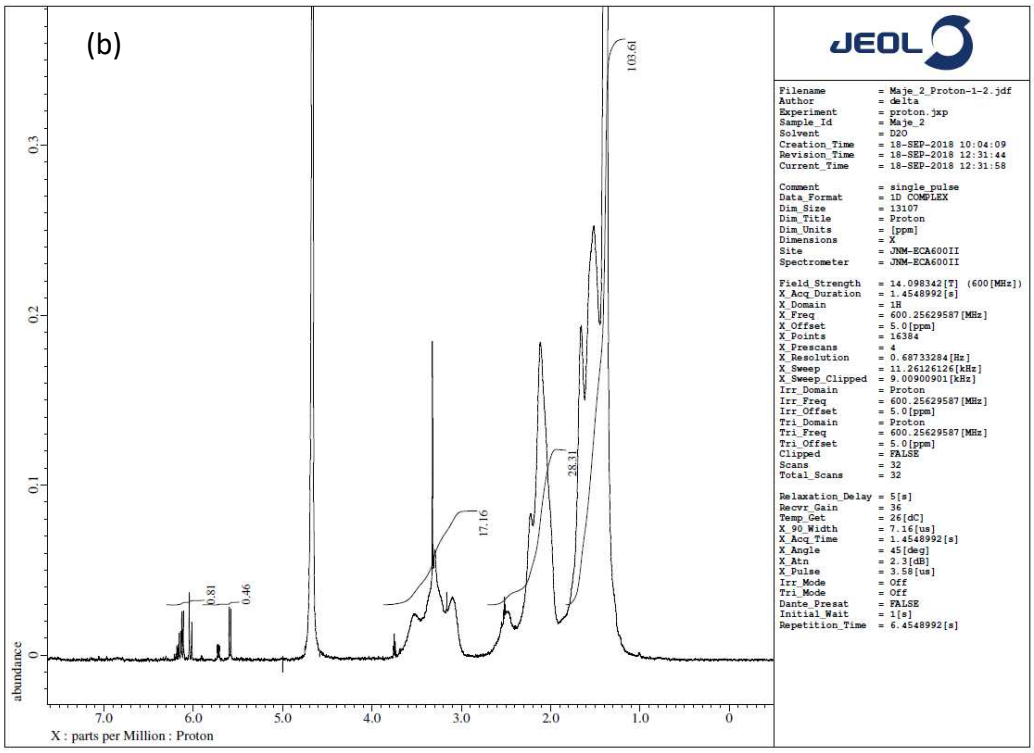
(b)
103.61
28.31
17.16
0.81
0.46
abundance
X : parts per Million : Proton
JEOL
Filename = Maje_2_Proton-1-2.jdf
Author = delta
Experiment = proton.jxp
Sample_Id = Maje_2
Solvent = D2O
Creation_Time = 18-SEP-2018 10:04:09
Revision_Time = 18-SEP-2018 12:31:44
Current_Time = 18-SEP-2018 12:31:58
Comment = single_pulse
Data_Format = 1D COMPLEX
Dim_Size = 13107
Dim_Title = Proton
Dim_Units = [ppm]
Dimensions = X
Site = JNM-ECA600II
Spectrometer = JNM-ECA600II
Field_Strength = 14.098342[T] (600[MHz])
X_Acq_Duration = 1.4548992[s]
X_Domain = 1H
X_Freq = 600.25629587[MHz]
X_Offset = 5.0[ppm]
X_Points = 16384
X_Prescans = 4
X_Resolution = 0.68733284[Hz]
X_Sweep = 11.26126126[kHz]
X_Sweep_Clipped = 9.00900901[kHz]
Irr_Domain = Proton
Irr_Freq = 600.25629587[MHz]
Irr_Offset = 5.0[ppm]
Tri_Domain = Proton
Tri_Freq = 600.25629587[MHz]
Tri_Offset = 5.0[ppm]
Clipped = FALSE
Scans = 32
Total_Scans = 32
Relaxation_Delay = 5[s]
Recvr_Gain = 36
Temp_Get = 26[dC]
X_90_Width = 7.16[us]
X_Acq_Time = 1.4548992[s]
X_Angle = 45[deg]
X_Atn = 2.3[dB]
X_Pulse = 3.58[us]
Irr_Mode = Off
Tri_Mode = Off
Dante_Presat = FALSE
Initial_Wait = 1[s]
Repetition_Time = 6.4548992[s]

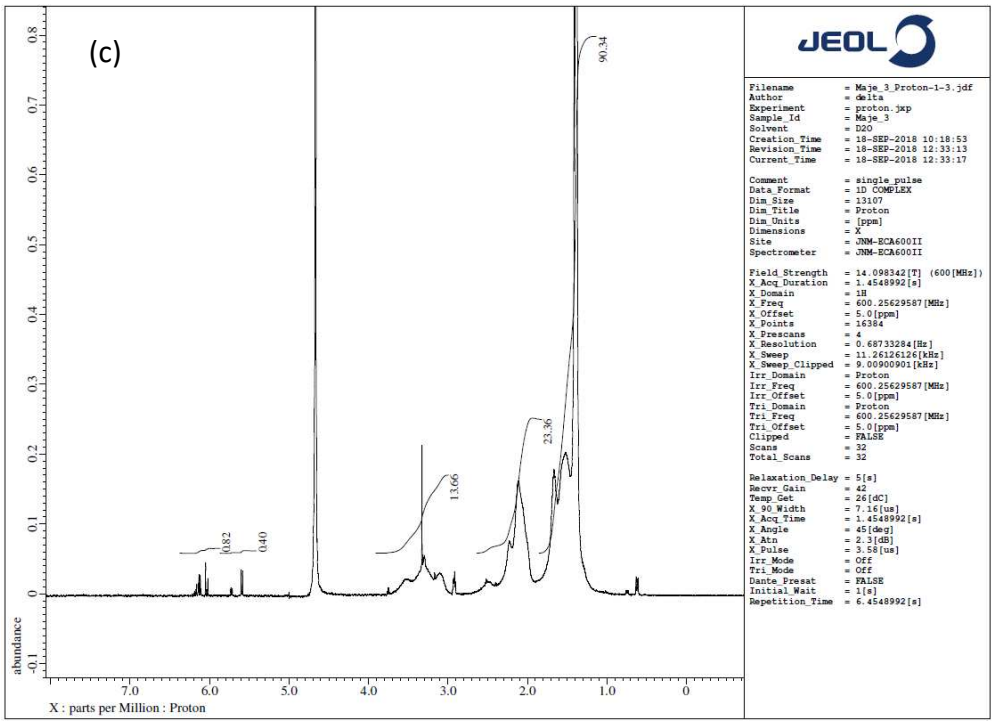

Figure 8. ^{1}H-NMR of (a) PAM, (b) SiO_2/PAM and (c) M_SiO_2/PAM solutions.

As illustrated in **Fig. 9a**, the chemical bonding between the NP-free PAM, SiO_2/PAM and M_SiO_2/PAM was investigated using ATR-FTIR spectroscopy to understand the formation mechanisms of the added NPs. The peaks at 2923, 2953, and 3321 cm^{-1} are attributed to the ring structure vibration of C–H stretching, O-H group and N-H group of the PAM amide chains, and the peak appeared at 1700 cm^{-1} is attributed to the C=O (carbonyl) functional groups of the polymer amides chain [26]. Correspondingly, the peak representing SO_3 group initiated from APSA monomer appeared at 1040 cm^{-1} [68, 69]. The peaks at 1480 and 1078 cm^{-1} in the M_SiO_2/PAM and SiO_2/PAM spectra represent Si–O–Si asymmetric bending and stretching vibrations, respectively, supporting the existence of hydrogen bond between the incorporated NPs and the PAM molecules [26]. However, in comparison to SiO_2/PAM, there is new broader peak appears between 2000 and 2500 cm^{-1} in M_SiO_2/PAM spectra, indicating the formation of the new electrostatic chemistry that occur when the additional proton (H^+) from the amino group of M_SiO_2 react with the polymer ionic charges, reinforced the ability of polymer

molecules to be adsorbed onto the M_SiO_2 NPs surface by ionic linkage as illustrated in **scheme 3.**

TGA was carried out using a heating range from 25 to 900 °C, with the TGA curves of the NP-free PAM, SiO_2/PAM and M_SiO_2/PAM shown in **Fig. 9b**. The TGA analysis demonstrated that M_SiO_2/PAM displayed a slight weight loss between 50 and 150 °C, which is attributed to the decomposition of attached APTES and desorption of water molecules from the surface. It can also be observed that, compared to NP-free PAM and SiO_2/PAM samples, the M_SiO_2/PAM composites show a small weight loss (~10%), indicating how fairly stable the M_SiO_2 NPs on the PAM surface, although the weight remains almost constant until 900 °C. However, the weight lost on SiO_2/PAM composites is roughly divided into three stages, at around 400 °C, almost 20% of the sample weight was lost, at around 700 °C around 12% loss was observed, and more than 3% weight loss was observed after heating to 900 °C, which is attributed to the decomposition of surface modified components on the polymer surface. Contrarily, the neat PAM shows significant loss of weight (~45%) until 350 °C, probably because of the loss of adsorbed water and slowly polymer decompositions, more weight loss followed on the same material to around 80% from 450 °C and above, which is because of ammonia evolution and chain scission of the polymer at high temperature. This finding is in agreement with the literature [70, 71]. However, the M_SiO_2/PAM composites have high temperature durability because they possesses additional covalent bond and stronger coordination bonds between the PAM backbone and the M_SiO_2, compared to SiO_2/PAM which only has hydrogen bonding on the surface, this makes M_SiO_2/PAM more temperature resistance than the other samples.

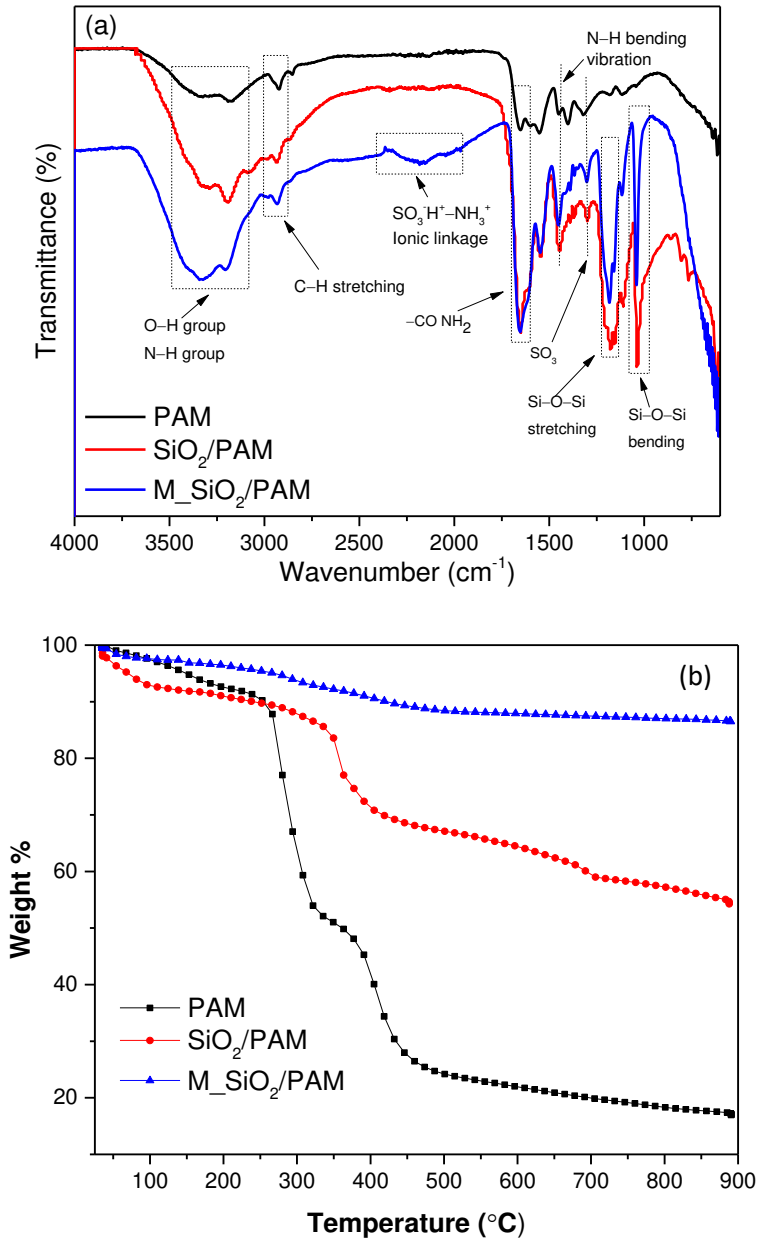

Figure 9. (a) ATR-FTIR spectra of NP-free PAM, SiO_2/PAM and M_SiO_2/PAM **(b).** TGA profiles of NP-free PAM, SiO_2/PAM and M_SiO_2/PAM nanocomposites

3.4. Effect of electrolyte on polymers viscosity

When PAM are dissolved in water, their carbonyl groups repel one another, resulting in the polymer structure to extent increasing the molecular chain hydrodynamic volume to which consequently improves the solution viscosity. Whereas, presence of excessive salinity in the water deteriorate the polymer performance in PF-EOR. The viscosity and hydrodynamic size

of polyelectrolyte polymers, such as PAM, are highly responsive to electrolyte concentration, for example the ionic shielding on the amide group (–CO–NH_2) reduces the polymer chain repulsion. This causes the polymeric chains collapse and consequently reduces the molecular coil size and hence lower down the viscosity [12, 72]. At extreme salt content with divalent ions such as Mg^{+2} and Ca^{+2}, the polymer starts to precipitate and become coiled from the elongated state as shown in **scheme 2**.

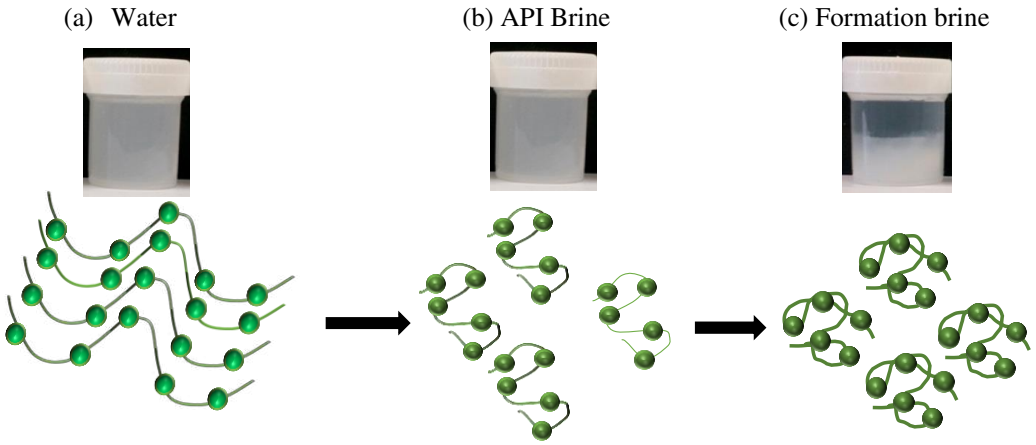

Scheme 2. Schematic illustration of the transformation from stretch to coiled or shrinkable state in the presence of (a) pure water (b) API brine and (c) Formation brine (details provide in **Table 4**).

In this section, the effect of electrolyte on the APV of NP-free PAM, SiO_2/PAM and M_SiO_2/PAM was investigated at 85 °C. **Fig. 10a** and **10b** presented the result of viscosity against the polymer type and shear rate (10-1000 S^{-1}), and **Table 5** illustrates the effect of API brine and formation brine (FB) on the viscosity decrease (percentage). The results shows that the addition of salt decreases the viscosity of all the three samples, this finding is similar to that reported in the literature [49, 73] where a reduction in viscosity was seen at high salinities. It can be said that when salt is introduced into the polymer, the cationic charge can neutralise the ionic charge of the polymer –CO–O^- groups, decreasing the electrostatic repulsions of the polymer chains to create a conformational transition from stretch to shrinkable or coiled state [74]. This causing the entanglement and hydrodynamic radius of the polymers to dissociate

which ultimately reduces the viscosity. M_SiO_2/PAM exhibit much stronger salt tolerance with higher viscosity compared to NP-free PAM and SiO_2/PAM in the presence of both API and FB. This is because the M_SiO_2/PAM has an additional positively charged active sites on the surface that can generate electrostatic repulsion between the polymer cationic groups.

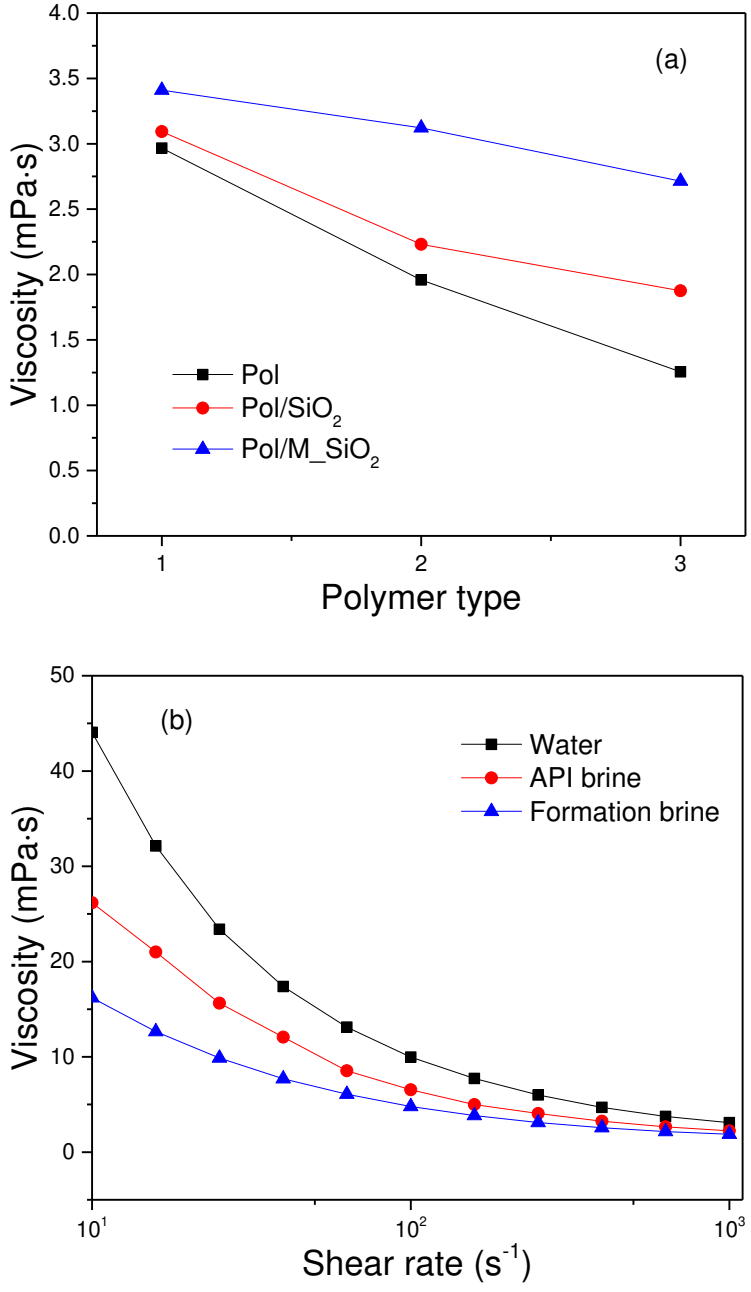

Figure 10. Influence of salinity on the viscosity of NP-free PAM, SiO_2/PAM and M_SiO_2/PAM to investigate the effect of (a) polymer type (where, 1= No salt, 2 = API brine 3 = Formation brine), and (b) effect of shear rate.

Table 5. Percentage of the remaining viscosity in the presence of FB and API brine

Sample	PAM	SiO_2/PAM	M_SiO_2/PAM
Pure	100 %	100 %	100 %
Formation brine	66%	72%	91%
API brine	42%	60%	80%

3.5. Effect of viscosity on the thermal stability of the polymers after long-term aging

Long-term aging under prolonged temperature and salinity results in detrimental effects in the PF-EOR, as it inhibits the overall performance of polymers by causing continuous viscosity reduction [26, 75]. It has been reported in the literature that most of the reservoirs that require EOR have high temperatures above 60 °C, and high-salinity (i.e. API standard (8 wt % NaCl and 2 wt % $CaCl_2$, which is equivalent to 1.8 M total ionic strength or >30000 mg/l) [26, 76, 77]. However, PAM could undergo significant reduction of viscosity when subjected to a certain [26, 78, 79]. The reduction would be caused by impairment of the hydrophobic effect due to the increased mobility of the polymer chains and the resultant loss of interchain liaisons [78, 79]. Therefore, the effect of aging under HT-HS conditions (80 °C and FB) has been investigated to highlight the influence of different polymers as shown in **Fig. 11a**. In the first instance, the results show a slight increase in the viscosity after one day aging in both SiO_2/PAM and M_SiO_2/PAM. This finding could be possibly due to the hydrolysis of the amide side chain of the polymer to its carboxylate group [26]; this shows that some part of the polymer carboxylate group could enhance the hydrodynamic volume. After 10 days aging M_SiO_2/PAM displayed better heat endurance capacity with 7.5% viscosity reduction, NP-free PAM and SiO_2/PAM with 41 and 28% reduction in viscosity, respectively. The viscosity of M_SiO_2/PAM dropped slightly until 30 days of aging while in NP-free PAM and SiO_2/PAM a sharp decrease was continued to be seen within the first month of aging. However, after 30 days of high temperature storage, the viscosity of the NP-free PAM continues to decline day by day. This is due to the effect of bridging anionic carboxylic groups of polymer with divalent

ions (Ca^{+2} and Mg^{+2}) and also polymer partial precipitation at high degree of hydrolysis [80]. Overall, M_SiO_2/PAM exhibits much stronger heat tolerance and stable viscosity compared to NP-free PAM and SiO_2/PAM over the whole period of aging, for instance, at 30 days PAM and SiO_2/PAM lost almost 51% and 41% of viscosity while M_SiO_2/PAM lost only 9.5%. After 90 days of aging the amount of viscosity lost is 10.5% for M_SiO_2/PAM and 78.7% and 45% viscosity reduction were observed for NP-free PAM and SiO_2/PAM. **Fig. 11b** shows consistent trends after calculating the relative viscosity of NP-free PAM, SiO_2/PAM and M_SiO_2/PAM, respectively.

The findings prove that introduction of SiO_2 NPs to acrylamide based polymers noticeably enhances the polymer thermal stability. Further improvement of the thermal properties was observed on M_SiO_2/PAM. The mechanism of thermal degradation and viscosity reduction of the polymer can be explained by two structural changes in the polymer molecule, both of which are caused by extreme temperature. First, carboxyl groups form by hydrolysing the amide chain and second, the polymer backbone scission lowers the viscosity [81]. When the carboxylic group content increases, the polymer molecules exhibit greater expansion state because of repulsion between negatively charge groups, and at the same time promote the polymer molecules interaction by creating a hydrogen bond betwixt the carboxyl and amide groups. Intermolecular and intramolecular interactions occur between the polymer molecules, this is interaction between different functional groups of the polymers which may lead to the formation of larger molecules and consequently increases the viscosity. A further interaction between functional groups of the same polymer may cause the polymer molecules to shrink and hence lowers the viscosity [11, 82, 83]. Many recent studies reported that introducing NPs in the polymer solutions could produce crosslinking networks of individual polymers and produce a solid hybrid system via the formation of hydrolysable covalent bond and hydrogen bond [26, 40]. For example, a remarkable increase in temperature stability and rheological

properties of acrylamide-based polymer was observed after SiO_2 NPs was introduced in the solution [84].

The proposed mechanism showing in **scheme 3**, shows a tremendous improvement in the polymer NPs interaction with the M_SiO_2 compared to pure SiO_2. This is because the M_SiO_2 surface has more functional groups, higher amino group reactivity, presence of more hydrogen in the amino groups and at the same time promote the formation of new electrostatic chemistry that occur when the additional proton (H^+) from amino group of M_SiO_2 react with the polymer ionic charges, reinforced the ability of polymer molecules to be adsorbed onto the M_SiO_2 NPs surface by ionic linkage as illustrated in **scheme 3**. This has also led to improved thermal stability of polymer backbone, polymer molecules, and polymer nanocomposites network. These results show that M_SiO_2/PAM show how M_SiO_2 could play a role in strengthened polymer molecular weight, ductility, and embrittlement, and greater efficiency to perform under harsh reservoir conditions.

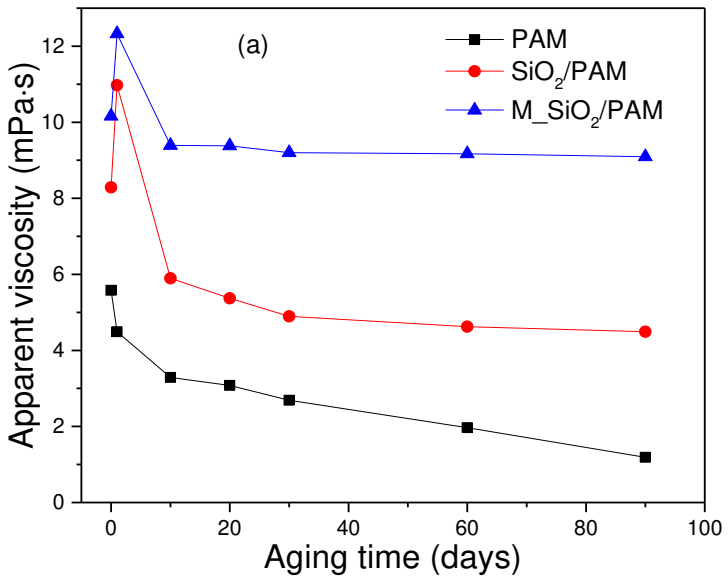

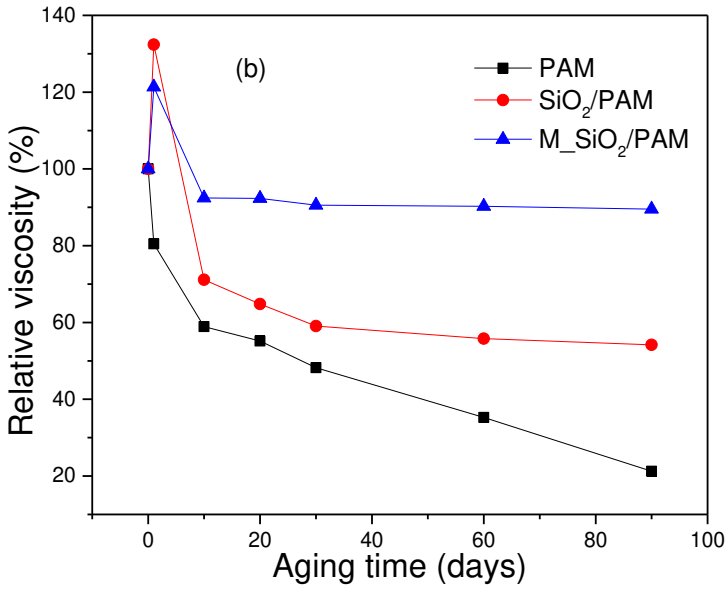

Figure 11. (a) Apparent viscosity (b) Relative viscosity as a function of aging time to investigate the effect of Long-term stability after 90 days at 85 °C, in the presence of FB.

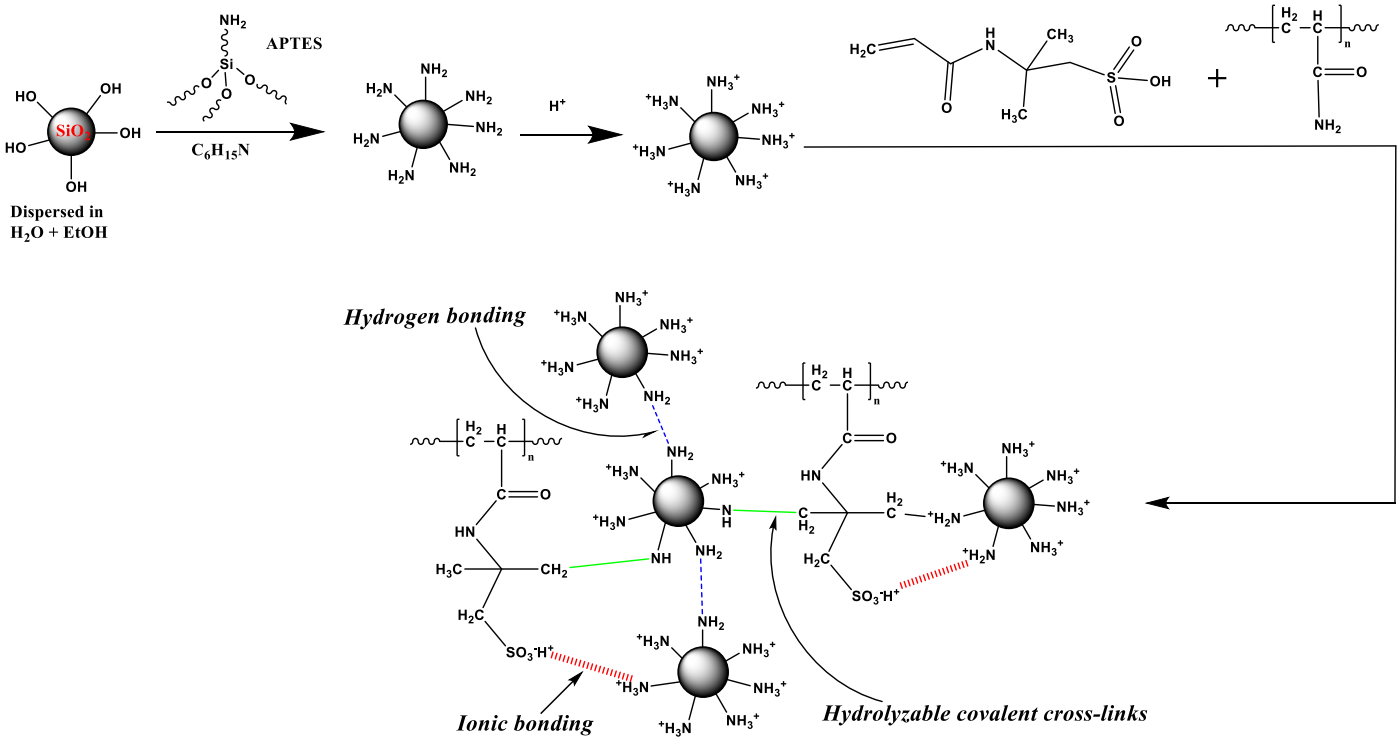

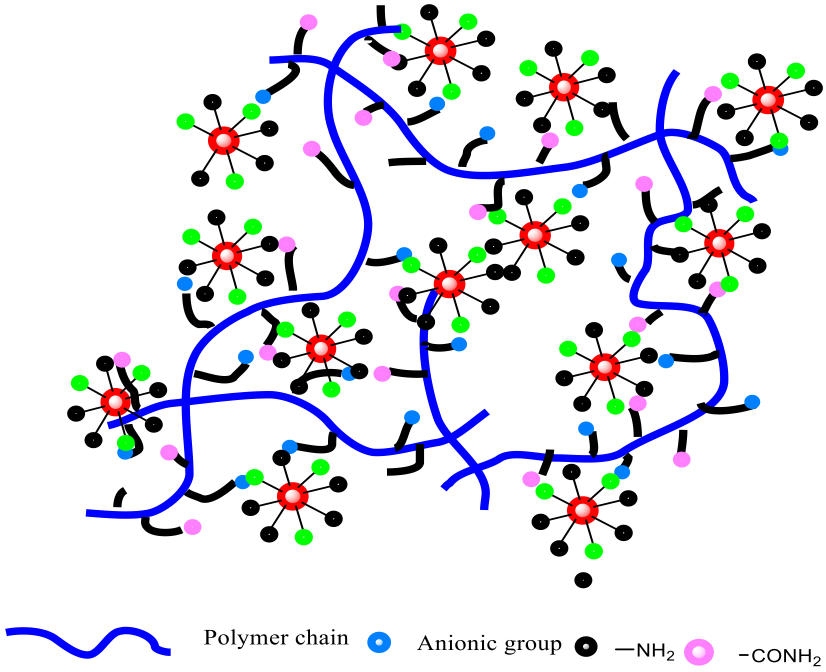

Scheme 3. Schematic representation of preparing M_SiO_2/PAM and potential interactions between polymer molecules and M_SiO_2 particles (top). Cartoons illustration of composites network system of Pol/M_SiO_2 (bottom).

3.5.1. Viscoelastic properties of the nanocomposites

In the PF process, it is important to examine the viscoelastic behaviour of the fluid in order to have a reasonable interpretation of the deformation character of the polymer structure [85-88]. Here, we have investigated the oscillatory behaviour of the polymers by measuring the changes in their loss modulus (G'') and storage modulus (G') as a function of angular frequency (ω). The results in **Fig. 12a** shows an increase in both G' and G'' with an increasing ω in all the three samples, however, at low ω the plateau of G' and G'' indicating the obvious solid-like behaviour of an elastic material and gel network nature of nanofillers in polymer composites and colloidal gels. Precisely, it could be noted that M_SiO_2/PAM samples show higher G' and G'' values exhibiting a better viscoelastic strength compared to SiO_2/PAM and NP-free PAM samples, respectively. This proves that the M_SiO_2 can reduce the relaxation of the polymer chain and change the effect of polymer liberation to become less obvious. **Fig. 12b** shows the

effect of complex viscosity (μ^*) of the composites against ω; the results obey similar changing trends as observed for G' and G''. The μ^* of pure polymer and SiO_2/PAM is lower than that of M_SiO_2/PAM. This finding shows the potential of using amino M_SiO_2 as a potential agent in improving the polymer performance in EOR.

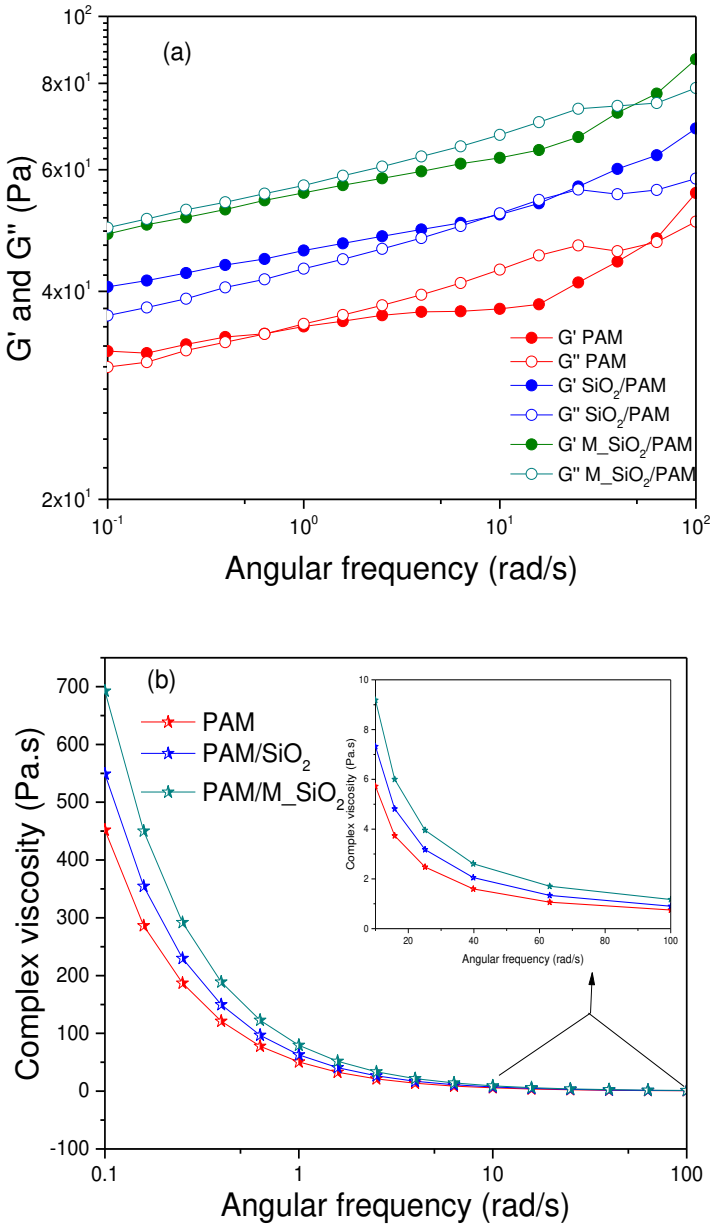

Figure 12. (a) Storage modulus (G') and loss modulus (G") and (b) complex viscosity of NP-free PAM, a SiO_2/PAM and M_SiO_2/PAM versus angular frequency (ω).

3.6. Enhanced oil recovery test

Increasing reservoirs sweep efficiency is the most important aspect in PF-EOR [2-5]. This technique is based on altering the mobility ratio between oil and injection fluid by the addition of polymers to improve vertical and areal sweep efficiencies and thereby reducing viscous fingering [21, 73]. Notwithstanding, the PF efficiency is affected by several situations including pore throats blockage because of the polymer aggregation [9, 10], polymer degradation with the influence of extreme temperature and salinity conditions [11-15] and polymer adsorption onto the surface of the porous media [16, 17], these hinder the PF performance, causing huge economic expenditures and severe viscosity reduction. In this section, a series of six core-flooding experiments were employed to examine the effect of NP-free PAM, SiO_2/PAM and M_SiO_2/PAM on the incremental oil recovery HT-HS conditions (**Table 4**). The experimental conditions and the comparisons of overall oil recoveries are tabulated in **Table 6,** and the obtained results of the accumulated oil recovery are shown in **Fig. 13.** The first 3 set of experiment was conducted using API brine at 85 °C, after injecting 3.0 PV of brine solution for each experiment around 50-52% of the oil was recovered relative to the original oil in place (OOIP), meaning that around 48-50% of the OOIP remain unrecovered by the means of conventional water flooding. Consequently, the overall oil recovery increase was 7.7% and 12.7% after NP-free PAM and SiO_2/PAM injection, while 17.5% increase of oil recovery was obtained after M_SiO_2/PAM injection under the same condition. A similar trend of oil recovery was recorded under after using FB at the similar temperature with overall oil recovery increase of 6.2% and 9.6% for NP-free PAM and SiO_2/PAM, whereas 16.2% oil were recovered after injecting M_SiO_2/PAM solution, lower than that of API brine samples.

The primary reason for a greater oil recovery by M_SiO_2/PAM is the ability of the M_SiO_2 to alter the oil/water mobility ratio. This could be associated to the higher viscosity and improved

stability after long-term ageing at high temperature demonstrating higher ability to be implemented under HT-HS without much decrease in viscosity. The M_SiO_2/PAM also shows greater performance due to its fair viscous force when injected into the core, but the other two samples especially NP-free PAM were believed to reduce their viscosity at HT-HS conditions because of poor stability. Thus, the highly stable solution could sweep the major core area without blocking the pores which makes more oil recovery to be achieved. These improved properties of M_SiO_2/PAM were generated due to the incorporated amino functional groups presence on the surface of added NPs, which results in the evolution of new electrostatic chemistry that occur when the additional proton (H^+) from the amino group of M_SiO_2 react with the polymer ionic charges, reinforced the ability of polymer molecules to be adsorbed onto the M_SiO_2 NPs surface. During the core-flooding experiment, the differential pressure was recorded for all the tests as seen in **Fig. 14**. The pressure drop increases after injecting the PAM and SiO_2/PAM samples in both conditions, this might be due to the log-jamming caused by aggregation and instability of the solution. While M_SiO_2/PAM composites sample showed better pressure drop which occur as a results of better stability caused by surface modification to create positively charged active groups that enhanced a stronger interaction with PAM functional groups, leading to high dispersion stability. These could reduce the energy required during the injection which greatly increases the potential for future field applications.

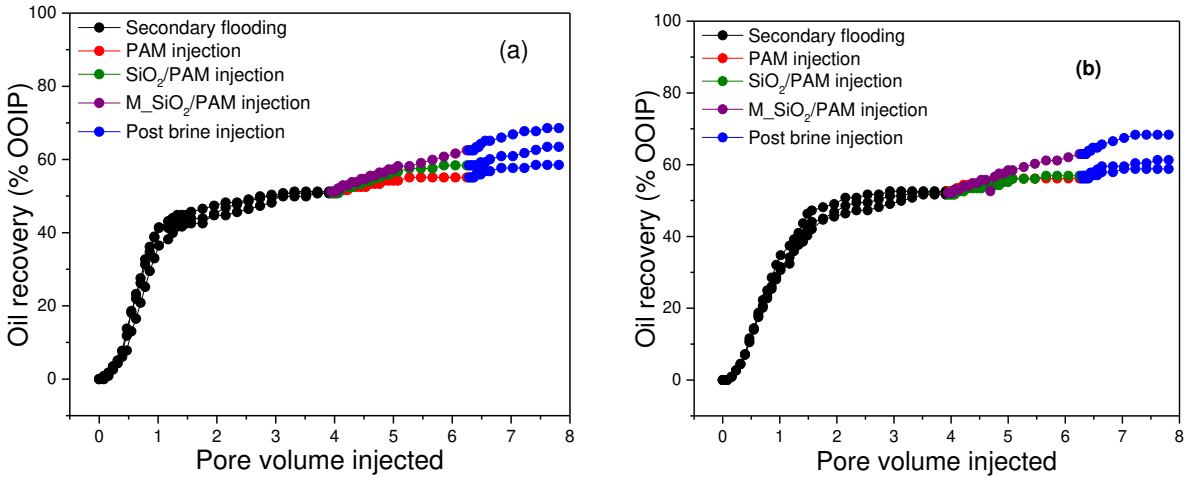

Figure 13. Tertiary oil recovery for NP-free PAM, SiO_2/PAM and M_SiO_2/PAM at HT-HS conditions (a) API brine and (b) FB brine, the temperature used for these test is 80 °C throughout.

Table 6. Oil recovery efficiency for NP-free PAM, SiO_2/PAM and M_SiO_2/PAM at HT-HS conditions (a) API brine and (b) FB brine

Displacing Fluid		NP-free PAM	SiO_2/PAM	M_SiO_2/PAM
(a)	Efficiency after brine flooding, % OOIP	50.77	50.76	51.21
	Efficiency after tertiary flooding, % OOIP	55.07	58.38	62.50
	Efficiency after post brine flooding, % OOIP	58.93	63.45	68.57
	EOR by sample, % OOIP	4.30	7.61	11.28
	EOR by chase water, % OOIP	3.44	5.08	6.18
	Overall oil recovery, % OOIP	7.74	12.68	17.46
(b)	Efficiency after brine flooding, % OOIP	52.58	51.66	52.16
	Efficiency after tertiary flooding, % OOIP	56.58	56.92	62.05
	Efficiency after post brine flooding, % OOIP	58.82	61.30	67.44
	EOR by sample, % OOIP	3.56	5.23	10.79
	EOR by chase water, % OOIP	2.67	4.37	5.40
	Overall oil recovery, % OOIP	6.23	9.60	16.20

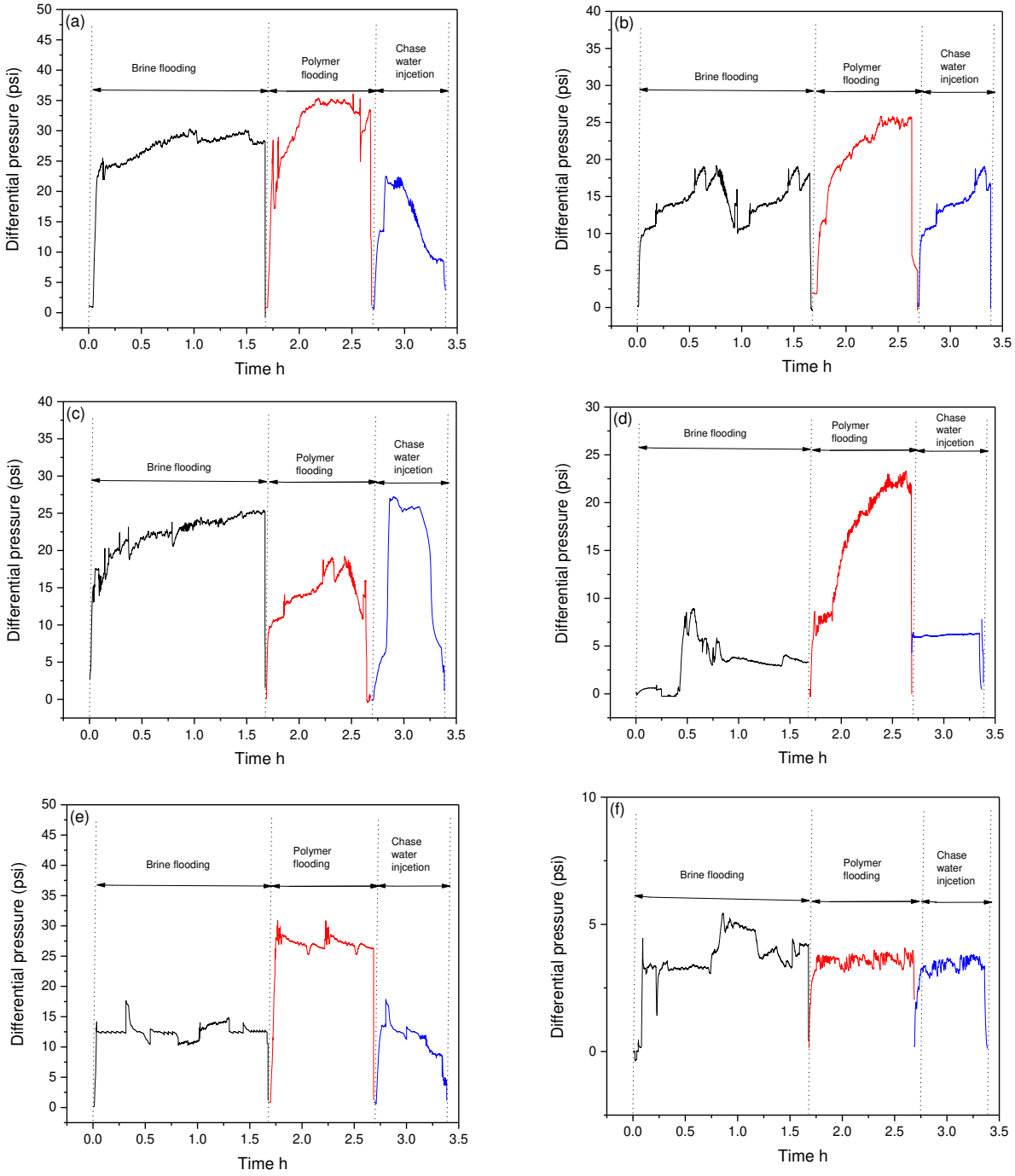

Figure 14. The Differential pressure for (a) PAM flooding (b) PAM_SiO_2 flooding (c) PAM_M_SiO_2 flooding in the presence of API brine and (d) PAM flooding (e) PAM_SiO_2 flooding (f) PAM_M_SiO_2 flooding in the presence of formation brine.

4. Conclusions

In this study, SiO_2 NPs were successfully functionalised with (3-aminopropyl) triethoxysilane to create positively charged active sites on the surface to form a stable NP dispersion, which facilitates the formation of strong coordination bond with the negatively charged PAM chain. Three samples including M_SiO_2/PAM, SiO_2/PAM and NP-free PAM were synthesised *in-situ* via free radical polymerisation, and their thermal degradation, variations of apparent viscosity and effect of aging time were investigated. The outcome of the finding revealed that M_SiO_2 could inhibit thermal degradation of the polymer and safeguard its backbone to prevent the polymer molecule from rupture under HT-HS conditions. As a result, M_SiO_2/PAM possessed excellent temperature tolerance and thermal stability at harsh environment. While SiO_2/PAM and NP-free PAM had 45 and 78% viscosity reduction respectively after 90 days of aging, only 10% reduction was observed in M_SiO_2/PAM. Our flooding experiments showed that M_SiO_2/PAM solution provided more oil recovery than those from SiO_2/PAM and NP-free PAM solutions in HT-HS conditions. These improved properties of M_SiO_2/PAM were generated due to the incorporation of amino functional groups on the surface of the SiO_2 NPs, which result in the formation of electrostatic attraction that reinforced the bonding of PAM molecules with M_SiO_2.

Acknowledgment

The authors would like to thank the support of Petroleum Technology Development Funds (PTDF) in Nigeria, and the European Research Council (ERC-2014-CoG, Project reference: 648375).

Conflicts of interest

The authors declare no conflict of interest.

List of nomenclatures

Full name	Symbol
Enhanced oil recovery	EOR
Polymer flooding	PF
Polyacrylamide	PAM
High temperature-High salinity	HT-HS
Nanoparticles	NPs
Silicon dioxide	SiO_2
Modified silicon dioxide	M_SiO_2
2-Acrylamido-2-methyl-1-propanesulfonic acid	APSA
acrylamide	AA
4-4'-azo-bis-4-cyanopentanoic acid	ACPA
Polydimethylsiloxane, (3-Aminopropyl)triethoxysilane	APTES
Triethylamine	TEA
Near-infrared	NIR
Particle size distribution	PSD
Dynamic light scatting	DLS
Nuclear magnetic resonance	NMR
Thermogravimetric analysis	TGA
attenuated total reflection-Fourier transform infrared	ATR-FTIR
Scanning electron microscope	SEM
Transmission electron microscope	TEM
Energy dispersive X-ray spectrometer	EDX
Gel permeation chromatography	GPC
Discovery hybrid rheometer	DHR
Relative viscosity	RV
Apparent viscosity	AV
American petroleum institute	API
API Brine	AB
Formation brine	FB
Original oil in place	OOIP

References

1. Smalley, R.E., *Future global energy prosperity: the terawatt challenge.* Mrs Bulletin, 2005. **30**(06): p. 412-417.
2. Hashemi, R., N.N. Nassar, and P.P. Almao, *Nanoparticle technology for heavy oil in-situ upgrading and recovery enhancement: Opportunities and challenges.* Applied Energy, 2014. **133**: p. 374-387.

3. Kulicke, W.-M., et al., *Effect of molecular weight and molecular weight distribution on the rheological properties of aqueous poly (ethylene oxide) solution.* polymer bulletin, 1983. **9**(4): p. 190-197.
4. Needham, R.B. and P.H. Doe, *Polymer flooding review.* Journal of Petroleum Technology, 1987. **39**(12): p. 1,503-1,507.
5. Sheng, J.J., B. Leonhardt, and N. Azri, *Status of polymer-flooding technology.* Journal of Canadian Petroleum Technology, 2015. **54**(02): p. 116-126.
6. Pu, W., et al., *Synthesis and characterization of hyperbranched associative polyacrylamide.* RSC Advances, 2016. **6**(45): p. 39522-39529.
7. Wever, D., F. Picchioni, and A. Broekhuis, *Polymers for enhanced oil recovery: a paradigm for structure–property relationship in aqueous solution.* Progress in Polymer Science, 2011. **36**(11): p. 1558-1628.
8. Thomas, A., N. Gaillard, and C. Favero, *Some key features to consider when studying acrylamide-based polymers for chemical enhanced oil recovery.* Oil & Gas Science and Technology–Revue d'IFP Energies nouvelles, 2012. **67**(6): p. 887-902.
9. Green, D.W. and G.P. Willhite, *Enhanced oil recovery*. Vol. 6. 1998: Henry L. Doherty Memorial Fund of AIME, Society of Petroleum Engineers Richardson, TX.
10. Sorbie, K.S., *Polymer-improved oil recovery*. 2013: Springer Science & Business Media.
11. Caulfield, M.J., et al., *Degradation on polyacrylamides. Part I. Linear polyacrylamide.* Polymer, 2003. **44**(5): p. 1331-1337.
12. Muller, G., J. Fenyo, and E. Selegny, *High molecular weight hydrolyzed polyacrylamides. III. Effect of temperature on chemical stability.* Journal of Applied Polymer Science, 1980. **25**(4): p. 627-633.
13. Pu, W., et al., *Synthesis and evaluation of β-cyclodextrin-functionalized hydrophobically associating polyacrylamide.* RSC Advances, 2016. **6**(98): p. 96006-96014.
14. Ramsden, D. and K. McKay, *The degradation of polyacrylamide in aqueous solution induced by chemically generated hydroxyl radicals: Part II—Autoxidation of Fe2+.* Polymer degradation and stability, 1986. **15**(1): p. 15-31.
15. Seright, R., *Potential for polymer flooding reservoirs with viscous oils.* SPE Reservoir Evaluation & Engineering, 2010. **13**(04): p. 730-740.
16. Ali, M. and H.B. Mahmud. *The effects of concentration and salinity on polymer adsorption isotherm at sandstone rock surface*. in *IOP Conference Series: Materials Science and Engineering*. 2015. IOP Publishing.
17. Clarke, A., et al., *Mechanism of anomalously increased oil displacement with aqueous viscoelastic polymer solutions.* Soft Matter, 2015. **11**(18): p. 3536-3541.
18. Lai, N., et al., *A water-soluble acrylamide hydrophobically associating polymer: Synthesis, characterization, and properties as EOR chemical.* Journal of Applied Polymer Science, 2013. **129**(4): p. 1888-1896.
19. Raffa, P., A.A. Broekhuis, and F. Picchioni, *Polymeric surfactants for enhanced oil recovery: A review.* Journal of Petroleum Science and Engineering, 2016. **145**: p. 723-733.
20. Sarsenbekuly, B., et al., *Study of salt tolerance and temperature resistance of a hydrophobically modified polyacrylamide based novel functional polymer for EOR.* Colloids and Surfaces A: Physicochemical and Engineering Aspects, 2017. **514**: p. 91-97.
21. Chen, Q., et al., *Thermoviscosifying polymer used for enhanced oil recovery: rheological behaviors and core flooding test.* Polymer bulletin, 2013. **70**(2): p. 391-401.
22. Deng, Y., et al., *Bonding between polyacrylamide and smectite.* Colloids and Surfaces A: Physicochemical and Engineering Aspects, 2006. **281**(1-3): p. 82-91.
23. Roustaei, A., S. Saffarzadeh, and M. Mohammadi, *An evaluation of modified silica nanoparticles' efficiency in enhancing oil recovery of light and intermediate oil reservoirs.* Egyptian Journal of Petroleum, 2013. **22**(3): p. 427-433.

24. Karimi, A., et al., *Wettability alteration in carbonates using zirconium oxide nanofluids: EOR implications.* Energy & Fuels, 2012. **26**(2): p. 1028-1036.
25. El-Diasty, A.I. and A.M. Aly. *Understanding the mechanism of nanoparticles applications in enhanced oil recovery*. in *SPE North Africa Technical Conference and Exhibition*. 2015. Society of Petroleum Engineers.
26. Hu, Z., et al., *Rheological Properties of Partially Hydrolyzed Polyacrylamide Seeded by Nanoparticles.* Industrial & Engineering Chemistry Research, 2017. **56**(12): p. 3456-3463.
27. Nourafkan, E., et al., *Improved rheological properties and stability of multiwalled carbon nanotubes/polymer in harsh environment.* Journal of Applied Polymer Science, 2018: p. 47205.
28. Haruna, M.A., et al., *Influence of carbon quantum dots on the viscosity reduction of polyacrylamide solution.* 2019. **248**: p. 205-214.
29. Singh, S.K., R.M. Ahmed, and F. Growcock. *Vital role of nanopolymers in drilling and stimulations fluid applications*. in *SPE Annual Technical Conference and Exhibition*. 2010. Society of Petroleum Engineers.
30. Kamal, M.S., et al., *Recent advances in nanoparticles enhanced oil recovery: rheology, interfacial tension, oil recovery, and wettability alteration.* Journal of Nanomaterials, 2017. **2017**.
31. Ershadi, M., et al., *Carbonate and sandstone reservoirs wettability improvement without using surfactants for Chemical Enhanced Oil Recovery (C-EOR).* Fuel, 2015. **153**: p. 408-415.
32. Nourafkan, E., et al., *Nanoparticle Formation in Stable Microemulsions for Enhanced Oil Recovery Application.* 2019. **58**(28): p. 12664-12677.
33. Wasan, D.T. and A.D. Nikolov, *Spreading of nanofluids on solids.* Nature, 2003. **423**(6936): p. 156-159.
34. Li, S., et al. *Effect of silica nanoparticles adsorption on the wettability index of Berea sandstone*. in *Paper SCA2013-059 presented at the international symposium of the society of core analysts held in Napa Valley, California, USA*. 2013.
35. Maghzi, A., et al., *Monitoring wettability alteration by silica nanoparticles during water flooding to heavy oils in five-spot systems: A pore-level investigation.* Experimental Thermal and Fluid Science, 2012. **40**: p. 168-176.
36. Maghzi, A., et al., *The impact of silica nanoparticles on the performance of polymer solution in presence of salts in polymer flooding for heavy oil recovery.* Fuel, 2014. **123**: p. 123-132.
37. Pillai, P., et al., *Effect of synthesized lysine-grafted silica nanoparticle on surfactant stabilized O/W emulsion stability: Application in enhanced oil recovery.* Journal of Petroleum Science and Engineering, 2019. **177**: p. 861-871.
38. Frijters, S., F. Günther, and J. Harting, *Effects of nanoparticles and surfactant on droplets in shear flow.* Soft Matter, 2012. **8**(24): p. 6542-6556.
39. Suleimanov, B., F. Ismailov, and E. Veliyev, *Nanofluid for enhanced oil recovery.* Journal of Petroleum Science and Engineering, 2011. **78**(2): p. 431-437.
40. Zhu, D., et al., *Aqueous hybrids of silica nanoparticles and hydrophobically associating hydrolyzed polyacrylamide used for EOR in high-temperature and high-salinity reservoirs.* Energies, 2014. **7**(6): p. 3858-3871.
41. Haruna, M.A., et al., *Improved rheology and high-temperature stability of hydrolyzed polyacrylamide using graphene oxide nanosheet.* Journal of Applied Polymer Science, 2019: p. 47582.
42. Haruna, M.A., et al., *Improved Polymer Flooding in Harsh Environment by Free-Radical Polymerization and the Use of Nanomaterials.* Energy & Fuels, 2019.

43. Ye, Z., et al., *Synthesis and performance of an acrylamide copolymer containing nano-SiO 2 as enhanced oil recovery chemical.* Journal of Chemistry, 2013. **2013**.
44. Bhardwaj, P., et al., *Nanosize polyacrylamide/SiO2 composites by inverse microemulsion polymerization.* International Journal of Polymeric Materials, 2008. **57**(4): p. 404-416.
45. Giraldo, L.J., et al., *The effects of SiO2 nanoparticles on the thermal stability and rheological behavior of hydrolyzed polyacrylamide based polymeric solutions.* Journal of Petroleum Science and Engineering, 2017. **159**: p. 841-852.
46. Portehault, D., et al., *Hybrid thickeners in aqueous media.* Colloids and Surfaces A: Physicochemical and Engineering Aspects, 2006. **278**(1-3): p. 26-32.
47. Petit, L., et al., *Responsive hybrid self-assemblies in aqueous media.* Langmuir, 2007. **23**(1): p. 147-158.
48. LeBaron, P.C., Z. Wang, and T.J. Pinnavaia, *Polymer-layered silicate nanocomposites: an overview.* Applied clay science, 1999. **15**(1-2): p. 11-29.
49. Zhu, D., et al., *Enhancing rheological properties of hydrophobically associative polyacrylamide aqueous solutions by hybriding with silica nanoparticles.* Journal of Applied Polymer Science, 2014. **131**(19).
50. Okay, O. and W. Oppermann, *Polyacrylamide− Clay Nanocomposite Hydrogels: Rheological and Light Scattering Characterization.* Macromolecules, 2007. **40**(9): p. 3378-3387.
51. Oberdisse, J., *Aggregation of colloidal nanoparticles in polymer matrices.* Soft matter, 2006. **2**(1): p. 29-36.
52. Wang, X., et al., *Facile surface modification of silica nanoparticles with a combination of noncovalent and covalent methods for composites application.* Composites Science and Technology, 2014. **104**: p. 1-8.
53. Graham, T., *XIV. On the properties of silicic acid and other analogous colloidal substances.* Proceedings of the Royal Society of London, 1864. **13**: p. 335-341.
54. Aalaie, J., *Rheological behavior of polyacrylamide/laponite nanoparticle suspensions in electrolyte media.* Journal of Macromolecular Science, Part B, 2012. **51**(6): p. 1139-1147.
55. Rahman, I.A. and V. Padavettan, *Synthesis of silica nanoparticles by sol-gel: size-dependent properties, surface modification, and applications in silica-polymer nanocomposites—a review.* Journal of Nanomaterials, 2012. **2012**: p. 8.
56. Zuniga, C.A., et al., *Long-Term High-Temperature Stability of Functionalized Graphene Oxide Nanoplatelets in Arab-D and API Brine.* ACS applied materials & interfaces, 2016. **8**(3): p. 1780-1785.
57. Hondow, N., et al., *Quantitative characterization of nanoparticle agglomeration within biological media.* Journal of Nanoparticle Research, 2012. **14**(7): p. 977.
58. Simon, A., et al., *Study of two grafting methods for obtaining a 3-aminopropyltriethoxysilane monolayer on silica surface.* Journal of colloid and interface science, 2002. **251**(2): p. 278-283.
59. Al-Oweini, R. and H. El-Rassy, *Synthesis and characterization by FTIR spectroscopy of silica aerogels prepared using several Si (OR) 4 and R'' Si (OR') 3 precursors.* Journal of Molecular Structure, 2009. **919**(1-3): p. 140-145.
60. Zhang, H., et al., *In situ synthesis of poly (methyl methacrylate)/SiO 2 hybrid nanocomposites via Grafting Onto strategy based on UV irradiation in the presence of iron aqueous solution.* Journal of Nanomaterials, 2012. **2012**: p. 3.
61. Lin, B. and S. Zhou, *Poly (ethylene glycol)-grafted silica nanoparticles for highly hydrophilic acrylic-based polyurethane coatings.* Progress in Organic Coatings, 2017. **106**: p. 145-154.
62. Ranjan, R. and W.J. Brittain, *Combination of living radical polymerization and click chemistry for surface modification.* Macromolecules, 2007. **40**(17): p. 6217-6223.

63. Walter, J., et al., *New possibilities of accurate particle characterisation by applying direct boundary models to analytical centrifugation.* Nanoscale, 2015. **7**(15): p. 6574-6587.
64. Chiu, H.-T., et al., *Using analytical centrifugation to characterize the dispersibility and particle size distributions of organic/inorganic composite coatings.* Journal of Polymer Research, 2011. **18**(6): p. 1587-1596.
65. Bergström, L., C.H. Schilling, and I.A. Aksay, *Consolidation behavior of flocculated alumina suspensions.* Journal of the American Ceramic Society, 1992. **75**(12): p. 3305-3314.
66. Lange, F. and K. Miller, *PRESSURE FILTRATION: CONSOLIDATION KINETICS AND MECHANICS.* AM. CERAM. SOC. BULL. Am. Ceram. Soc. Bull., 1987. **66**(10): p. 1498.
67. Alhreez, M. and D. Wen, *Controlled releases of asphaltene inhibitors by nanoemulsions.* Fuel, 2018. **234**: p. 538-548.
68. Durmaz, S. and O. Okay, *Acrylamide/2-acrylamido-2-methylpropane sulfonic acid sodium salt-based hydrogels: synthesis and characterization.* Polymer, 2000. **41**(10): p. 3693-3704.
69. Rosa, F., J. Bordado, and M. Casquilho, *Hydrosoluble copolymers of acrylamide-(2-acrylamido-2-methylpropanesulfonic acid). Synthesis and characterization by spectroscopy and viscometry.* Journal of applied polymer science, 2003. **87**(2): p. 192-198.
70. Dong, A., et al., *Synthesis of N-halamine-functionalized silica–polymer core–shell nanoparticles and their enhanced antibacterial activity.* Nanotechnology, 2011. **22**(29): p. 295602.
71. Gao, Y., Y. Hu, and K. Yao, *Surface molecularly imprinted polymers for solid-phase extraction of (–)-epigallocatechin gallate from toothpaste.* Frontiers of Chemical Science and Engineering, 2015. **9**(4): p. 467-478.
72. Al-Sabagh, A., et al., *Solution properties of hydrophobically modified polyacrylamides and their potential use for polymer flooding application.* Egyptian Journal of Petroleum, 2016. **25**(4): p. 433-444.
73. Jung, J.C., et al., *Rheology and polymer flooding characteristics of partially hydrolyzed polyacrylamide for enhanced heavy oil recovery.* Journal of Applied Polymer Science, 2013. **127**(6): p. 4833-4839.
74. Saito, S., *Salt effect on polymer solutions.* Journal of Polymer Science Part A-1: Polymer Chemistry, 1969. **7**(7): p. 1789-1802.
75. Pospíšil, J., et al., *Degradation and aging of polymer blends I. Thermomechanical and thermal degradation.* Polymer Degradation and Stability, 1999. **65**(3): p. 405-414.
76. Bagaria, H.G., et al., *Iron oxide nanoparticles grafted with sulfonated copolymers are stable in concentrated brine at elevated temperatures and weakly adsorb on silica.* ACS applied materials & interfaces, 2013. **5**(8): p. 3329-3339.
77. Saxena, N., A. Kumar, and A. Mandal, *Adsorption analysis of natural anionic surfactant for enhanced oil recovery: The role of mineralogy, salinity, alkalinity and nanoparticles.* Journal of Petroleum Science and Engineering, 2019. **173**: p. 1264-1283.
78. Kopperud, H.M., F.K. Hansen, and B. Nyström, *Effect of surfactant and temperature on the rheological properties of aqueous solutions of unmodified and hydrophobically modified polyacrylamide.* Macromolecular Chemistry and Physics, 1998. **199**(11): p. 2385-2394.
79. Shaikh, S., et al., *Synthesis and solution properties of poly (acrylamide-styrene) block copolymers with high hydrophobic content.* Polymer Engineering & Science, 1999. **39**(10): p. 1962-1968.
80. Gaillard, N., D.B. Sanders, and C. Favero. *Improved oil recovery using thermally and chemically protected compositions based on co-and ter-polymers containing acrylamide*. in *SPE improved oil recovery symposium*. 2010. Society of Petroleum Engineers.
81. Caulfield, M.J., G.G. Qiao, and D.H. Solomon, *Some aspects of the properties and degradation of polyacrylamides.* Chemical reviews, 2002. **102**(9): p. 3067-3084.

82. Xin, X., et al., *Interaction between sodium oleate and partially hydrolyzed polyacrylamide: A rheological study.* Colloids and Surfaces A: Physicochemical and Engineering Aspects, 2008. **326**(1-2): p. 1-9.
83. Chen, J., et al., *Fluorescence studies on hydrophobic associations of fluorocarbon-modified poly (acrylic acid) solutions.* Macromolecules, 1999. **32**(15): p. 4861-4866.
84. Maurya, N.K., P. Kushwaha, and A. Mandal, *Studies on interfacial and rheological properties of water soluble polymer grafted nanoparticle for application in enhanced oil recovery.* Journal of the Taiwan Institute of Chemical Engineers, 2017. **70**: p. 319-330.
85. Mitchell, J., et al., *Viscoelastic polymer flows and elastic turbulence in three-dimensional porous structures.* Soft matter, 2016. **12**(2): p. 460-468.
86. Spildo, K. and E.I. Sæ, *Effect of Charge Distribution on the Viscosity and Viscoelastic Properties of Partially Hydrolyzed Polyacrylamide.* Energy & Fuels, 2015. **29**(9): p. 5609-5617.
87. Wei, B., *Flow characteristics of three enhanced oil recovery polymers in porous media.* Journal of Applied Polymer Science, 2015. **132**(10).
88. ZHANG, L.-j. and X.-a. Yue, *Mechanism for viscoelastic polymer solution percolating through porous media.* Journal of Hydrodynamics, Ser. B, 2007. **19**(2): p. 241-248.